1-1-2003

Verification of a Lagrangian pollen dispersion model and sensitivity to particle size and environmental conditions

Jenny Marie Riese
Iowa State University

Verification of a Lagrangian pollen dispersion model and sensitivity to particle size and environmental conditions

by

Jenny Marie Riese

A thesis submitted to the graduate faculty

in partial fulfillment of the requirements for the degree of

MASTER OF SCIENCE

Major: Agricultural Meteorology

Program of Study Committee:
Raymond Arritt (Major Professor)
Eugene Takle
Mark Westgate

Iowa State University

Ames, IA

2003

Graduate College
Iowa State University

This is to certify that the master's thesis of

Jenny Marie Riese

has met the thesis requirements of Iowa State University

Signatures have been redacted for privacy

TABLE OF CONTENTS

CHAPTER 1. GENERAL INTRODUCTION

1.1 Introduction

Genetically modified crops (GMOs) are grown to improve taste and quality of food, while improving nutrients, increasing productivity and reducing the use of pesticides to develop sustainable agricultural practices (Institute of Food Science and Technology). There is concern, however, about possible unknown effects and consequences of genetically modified crops (Appell 2001; Foster et al. 2000). This concern exists because maize pollen travels through the air to pollinate the female flower.

This pollination occurs when pollen grains travel through the air to the silk and pollinate the female flower (located on the ear). Although more than one pollen grain can land on the silk and send pollen tubes to the ovary only one pollen grain fertilizes the egg cell, in the vast majority of cases. The probability of spore deposition over time depends on the probability of the spore encountering the vegetation and the probability of the vegetation capturing the spore (Aylor and Flesch 2001). Outcrossing occurs when a pollen grain from one maize plant pollinates a flower on another maize plant. In open-pollinated crops, such as maize, there is a need to predict the potential for outcrossing in a field, because of the need to control the flow of transgenes and the controversy over GMOs.

Currently there is insufficient knowledge to accurately predict the potential for outcross. The development of a pollen dispersion model will help determine the movement of pollen grains in response to wind direction and wind speed. This study uses a pollen dispersion model based on the Lagrangian statistical equation. When the Lagrangian pollen dispersion model is coupled with other biological and physical models it will help predict the amount of outcross in a field. An important component of developing such a model is to conduct sensitivity tests to determine how different

conditions affect the dispersion of pollen grains. Tests on pollen size, wind speed, and atmospheric stability are the subject of this thesis research.

Lagrangian model calculations are made on the moving particles not on a fixed grid. The Lagrangian model tracks the motions of particles released in the model (McNider 1981). A Lagrangian method is used so every pollen grain in the model can be tracked and identified by its source, time of release, and other properties of interest (such as the path it took to the ground or at what speed it traveled).

Previous work focused on either the physical or biological processes that affect pollen dispersion. Ashton et al. (2000) used a Gaussian air dispersion model that recreated the pollen deposition profile outside the maize field. Wilson (2000) studied dispersion of glass beads that were released from 7.42 m and 15.0 m and between 50 and 100 μm in size (same range as for pollen grains). He found that the leading edge of the deposition was located farther up-wind in unstable conditions than in neutral or stable conditions, and that the leading edge of deposition was farther up-wind in neutral conditions than in stable conditions.

A biological process that affects pollen is pollen viability. Luna et al. (2001) found that pollen exposed to warm, dry air loses 80% viability in one hour and 100% viability in two hours. Under more humid conditions, however, pollen viability was reduced by 58% after one hour, but was again reduced by 100% after two hours. Herrero and Johnson (1980) and Schoper et al. (1987) found that high temperatures during pollination could result in a poor kernel set, presumably due to loss of pollen viability.

Interactions of physical and biological processes include the timing of pollen shed, impact of weather on pollen dispersal and viability, and the competition between pollen grains from the local field and foreign fields to pollinate a kernel. There is a need to put the interactions together in a model to predict realistically the outcross of pollen grains. The pollen dispersion model will be one

of many submodels (for example: transport, viability, and risk assessment) combined to create a model able to predict maize growth, pollination, and risk assessment of outcrossing.

1.2 Thesis Organization

This thesis is organized in four sections: introduction, verification, results, and conclusions. Chapter one discusses the reason for making a Lagrangian pollen dispersion model. Chapter two discusses maize and how weather affects maize. Chapter three discusses the boundary layer, which is the layer of air just above the surface of the earth where pollen dispersion occurs.

The verification section is the verification of the Lagrangian pollen dispersion model with observations and comparisons with a Gaussian Model that has been previously used for pollen dispersion; this is done in chapter five.

The results section is how the Lagrangian pollen dispersion model reacts to sensitivity tests of pollen size (in chapter six) and atmospheric conditions of wind speed and atmospheric stability (in chapter seven).

The conclusions section is the final section of this thesis, and recaps the main points of each of the previous three sections.

CHAPTER 2. THE DEVELOPMENT OF MAIZE

2.1 How Maize Develops

This section discusses how the male (tassel) and female (ear) flowers of maize develop, anthesis (the release of pollen from the tassel), silk emergence (how and when the silk emerges from the ear), pollination and fertilization of the ear, and finally how meteorology can affect the development of maize. Figures 2.1, 2.2, and 2.3 show pictures of the parts of a maize plant, the tassel, and the ear respectively.

2.1.1 Floral Development

2.1.1.1 Staminate Inflorescence

Staminate (male) flower development begins with rachis (reproduction stem) formation of the tassel. Differentiation (going from one tassel to many tassels) begins when the top of the stem elongates and tassel branches appear at or near the base of the main (first) tassel (Kiesselbach 1999). Tassel branches differentiate individually, forming progressively higher on the tassel and on opposite sides of the main tassel rachis. The spikelets begin to form at the base of each branch and progress acropetally (beginning at the base and continuing upwards) to the apex of the rachis branch.

On each spikelet, two florets develop that are completely enclosed by a single pair of glumes, or leaves (a lemma and palea). See figure 2.4 for an example of a staminate flower. The lemma grows on the side adjacent the glume. Pistillate floret initials also form in each flower, but these degenerate quickly after they start to form; only the stamens continue to develop. One stamen develops near the lemma and two form opposite the palea. Two lodicules (which swell to allow for anthesis) develop near the base of the stamen over the lemma. Each stamen produces an anther supported by a filament.

Each anther has four loculi (or chambers) arranged on a central row of archesporial cells (which allow spore mother cells to develop). Within each loculi sporogenous tissue develop

(Kiesselbach 1999). The cells of the tissue divide into many cells called microspore mother cells. A cavity forms in the middle of the anther and the microspore mother cells form a single layer around this cavity.

The microspore mother cells are diploid (2n, containing two sets of ten chromosomes, one set from each parent). The microspore mother cells go through a process called meiosis (Kiesselbach 1999). In the first stage, diakinesis, the chromosomes shorten until they are approximately twice as long as they are wide. During telephase the chromosomes gather at opposite ends of the microspore mother cell. A microspore wall forms between the two ends during a nuclear division and starts the two-cell stage. During this time the cell goes through mitosis, where the cell divides into two cells and each of the cells are diploid. Again the two cells will go through the processes of diakinesis and telephase. When the cells divide into two again they go through meiosis (when the cell divides into two new cells they will have half the number of chromosomes than the original cell started with). The four nuclei are now haploid (1n = 10 chromosomes).

A microspore wall is organized around each of the four nuclei in the microspore mother cell. Cytoplasm becomes very dense in the microspore, or pollen grain, and the nucleus of each microspore divides into a vegetative and generative nucleus (Kiesselbach 1999). The generative nucleus then divides into two nuclei. The two generative nuclei are sperm cells that will pollinate the pistillate florets. These sperm cells are located inside the pollen grains that when released during anthesis can pollinate the ovaries of maize.

2.1.1.2 Pistillate Inflorescence

All nodes on the maize stem have the potential to form several axillary buds, but usually only one or two nodes near the middle of the plant will develop a rachis unit with mature pistillate flowers (the female flower). Each axillary bud is enclosed in a prophyllum, or modified leaf (Kiesselbach 1999). The axillary branch initially forms a number of leaves that will eventually surround the pistillate rachis (ear) as leaf husks. After the leaf initials have formed, floral structures begin to

differentiate. The growing point of the rachis then begins to elongate and form branches (Kiesselbach 1999). This aspect of development is similar to that of the tassel. When the leaf initiation stops, an apex forms branches upon which spikelets can form.

Initially the apex of the ear shoot is smooth. But rows of spikelet primordia soon begin to form. Rows of spikelets are produced in pairs by division of branch initials (Bonnett 1966). Each spikelet forms two florets, but in most cases, the basal floret degenerates leaving one floret per spikelet. Since spikelets develop from a division on a rachis branch, spikelets and their florets are always produced in pairs. So there is always an even number of floret rows around the mature rachis of maize. In cases where both of the florets develop, the rows may become irregular due to overcrowding (Kiesselbach 1999).

The apex of each floral shoot differentiates to form a functioning pistil (ovary and style). Three ring-like growths at the base of the pistil form carpels, which grow upward around the ovule and meet to form the pericarp at the stylar canal. This can be seen in figure 2.5. The two anterior carpels continue to develop into the style (silk), which will become layered with trichomes (developed from the cells of the epidermis) (Kiesselbach 1999). Very rarely the posterior carpel also takes part in forming the silk.

The sub-epidermal cell enlarges to become an archesporial cell, the megaspore mother cell. The megaspore mother cell undergoes meiosis in the same manner as the microspore mother cell, mentioned earlier, to form a quartet of megaspore cells. The apical megaspore cell persists to function as the first cell of the embryo sac; the other three cells degenerate.

The nucleus of the megaspore cell divides and a vacuole forms between the two nuclei. Both nuclei divide to form a group of four nuclei at polar ends of the embryo sac. One nucleus from each end migrates to the center of the embryo sac. These nuclei will join with one of the generative nuclei from the pollen to form the endosperm (see below). There are now three nuclei at the chalazal (apical) end and three nuclei at the micropylar (basal) end of the embryo sac. The three nuclei at the

chalazal end continue to divide until twenty to forty nuclei are formed. One of the three nuclei at the micropylar end enlarges to become the egg cell, which will be fertilized. The other two nuclei develop into synergids, which are thought to provide nutrients to the fertilized egg cell. The embryo sac is now mature and ready for fertilization. The embryo sac is an ovary on the ear of the maize plant.

2.1.2 Anthesis

The next step in pollination is release of the pollen from the anthers (anthesis). Anthesis occurs when the lodicules swell pushing the lemma and the palea apart allowing the anther to extend outside the glumes by the elongating filaments. The pollen is in the anther of the staminate floret. Upon exposure from the surrounding glumes the anthers dry and dehisce (break open) to release the mature pollen within. The majority of the pollen grains escape when winds shake the anthers. Small amounts of pollen are released under calm conditions. Under most conditions, all the pollen is released from an individual anther the same day it is exposed.

Generally, the tassel starts to shed the pollen shortly before the silks emerge from the pistillate flower, and pollen shed continues for several days. Pollen shed from the tassel begins at florets in the center of the central axis. The shedding progresses upward to the tip and downward to the base of the axis (Kiesselbach 1999). Florets in the tassel branches begin to shed after the central axis starts. Again, the shedding begins with central florets and progress up and down the branch.

Anthesis for a population is defined when 50% of the population has begun to shed pollen. The peak intensity of pollen shed occurs two to three days after anthesis. A typical peak pollen shed rate is approximately 700 grains cm^{-2} (Westgate and Lizaso, unpublished). The duration of the pollen shed (first pollen shed to the last pollen shed) is about 12 days for the population.

An input to the Lagrangian pollen dispersion model is the duration and intensity of pollen shed from the tassels. The model needs to know how many pollen grains and at what time the pollen grains are released so that it can predict the dispersion pattern of the pollen grains. Currently this

information is not known. The model uses estimated diurnal pollen shed percentages from Ashton et al. 2000 as shown later in chapter 4.

2.1.3 Silk Emergence

The carpels that merge together around the ovary of the pistillate flower form the silk. Cell elongation and division occurs over the entire length of the silk and the entire silk is receptive to pollen. Silk elongation occurs rapidly at first and then slows after the silks appear (Bassetti and Westgate 1993a). Seven to eight days after the silk emerges, the pistillate flower senesces and is no longer receptive to pollen.

Silks appear over a period of four to eight days (Bassetti and Westgate 1993a). Silk from florets in the lower third of the rachis are first to appear; silks from the basal and apical florets are generally the last to emerge (Bassetti and Westgate 1993a). The first silks to appear are also the first to senesce. Bassetti and Westgate (1993a) observed that the silks were receptive to pollen until the silks base is severely collapsed. In these senesced silks, the pollen tube cannot reach the ovary to fertilize the egg cell.

Bassetti and Westgate (1994) found that the earlier in the year the maize was planted the more silks would emerge from each ear. If silks emerge too early before anthesis they can senesce before the pollen has an opportunity to fertilize the ovary. If the silks emerge too late after anthesis the pollen could be gone before the silks emerge.

2.1.4 Pollination and Fertilization

The trichomes of the silk are very sticky and catch the pollen when it travels in the air. The silk supplies the pollen with moisture, which causes the pollen to germinate. The silk also provides the pollen tube with nutrients so that the tube can grow up to 25 cm to reach the embryo sac.

When the pollen grain germinates, the pollen tube emerges and elongates on the silk. As the pollen tube grows, it penetrates between the cells of the trichomes and enters the body of the silk (Kiesselbach 1999). The pollen tube grows within the transmitting tissues, which communicate with

the pollen tube to guide it towards the embryo sac. The pollen tube grows very rapidly (about 10 mm/h) until it reaches the micropylar end of the embryo sac.

Although more than one pollen grain can land on the silk and send pollen tubes to the ovary, in the vast majority of cases only one fertilizes the egg cell. Once the pollen tube reaches the embryo sac, it ruptures and releases the two sperm nuclei. One nucleus fuses with the nucleus of the egg cell to form a diploid embryo (zygote). Thus, the zygote contains one set of ten chromosomes from each of the two parents: one set from the female megaspore cell and one set from the male microspore. The other sperm nucleus fuses with the two nuclei in the center of the embryo sac to form the initial endosperm nucleus, which is triploid (3n). The endosperm nucleus contains two sets of chromosomes from the female megaspore, and one set of chromosomes from the male microspore. These nuclei proliferate rapidly to fill the endosperm cavity.

This process is called double fertilization because two fertilization events occur in the embryo sac. The first fertilization forms the zygote and a second fertilization forms the endosperm.

2.1.5 Interactions with Meteorology

Ideally, the silks begin to emerge within a day or two at the beginning of pollen shed (Bassetti and Westgate 1994). About 3000 pollen grains for every silk are required for maximum seed set (Westgate et al. 2003). Generally more pollen is produced than required for each plant (Westgate et al. 2003). Under normal conditions the fertilization occurs within 24 hours of pollination. When there is a drought and the silk water potential is low it can take twice as long (at least 48 hours) for the pollen to reach the embryo sac and fertilization to occur. Because of the longer time it takes the pollen to reach the embryo sac there is a lower kernel set due to the failure in the development of the ovary (Bassetti and Westgate 1993b).

Silk interaction with the environment is also very important. Bassetti and Westgate (1993b) found that silks had a slower elongation rate with less than normal water potential from too little water. They also found that water potential deficit in the early stages of floret development delayed

silk senescence. When water deficit was imposed later in floret development, silk senescence was accelerated. Thus water stress can decrease the number of silk available for pollination, as well as their receptivity to pollen.

2.2 Pollen Viability and Dispersion

This section describes pollen viability (how long the pollen stays viable and how weather conditions can affect the viability of pollen) and pollen dispersion (the time of day, where it disperses to, and what influences it).

2.2.1 Pollen Viability

There is a need to understand how meteorological conditions affect the viability of pollen. With drier conditions pollen viability decreases faster than under humid conditions. It remains unknown how fast the pollen viability decreases under changing meteorological conditions.

It is known that high temperatures during pollination can result in a poor kernel set. The optimum temperature for maize pollination is 30°C. As temperatures increase and percent germination decreases, the nonviable or nongerminated pollen increases (Herrero and Johnson, 1980). Heat tolerant hybrids had a larger percentage of anther emergence (64%) than heat intolerant hybrids (54%) and heat intolerant crossed with heat tolerant hybrids (57%) at higher temperatures (Schoper et al. 1987). Heat tolerant hybrids allow the pollen grains to remain variable at higher temperatures so the pollen grains can pollinate the ovary.

At anthesis, water comprises about 60% of the fresh weight of maize pollen (Luna et al. 2001). After it is released and moves through the air, the pollen dehydrates until it lands on the silk where the trichomes provide the pollen with water and nutrients. Pollen eventually loses viability as it dries; it must land on a silk soon after it is shed from the tassel to remain viable. Luna et al. (2001) found that pollen exposed to warm, dry air loses 80% viability in one hour and 100% viability in two hours. Under more humid conditions, however, pollen loses 58% viability in one hour, but again

loses by 100% viability in two hours. This contradicts Emberlin et al. (1999) who found that when maize pollen was kept dry for several days the pollen viability did not decrease. Some decrease in pollen viability may not affect the kernel set considering the tassels produce more pollen then needed. Research is needed to consider both the amount of pollen shed and pollen viability when the maize tassel is heat stressed.

The Lagrangian pollen dispersion model can be coupled with a pollen viability model to predict the percent of outcross of pollen grains in a field. If the pollen grains are no longer viable there is no chance for outcross; if the pollen grains are viable they need to compete with other pollen grains that landed on the same silk to pollinate the kernel. A pollen viability model can be used to predict the viability of the pollen grain and if the pollen grain is viable it will pollinate the kernel. The pollen viability model needs data to include how long the pollen grain has been in the air (the time it left the tassel to the time it landed on the silk) and what the weather conditions were while the pollen grain was in the air. The Lagrangian pollen dispersion model can output this information and so the pollen viability model may input the information.

2.2.2 Pollen Dispersion

Raynor et al. (1972) and Loubet et al. (2002) found that pollen grains are released when the wind speed increases and the air becomes drier during the morning. These studies found that more pollen grains are deposited inside the source field than outside the source field, and that more pollen grains are deposited closer to the source field than farther away from the source field. Raynor et al. (1972) found that pollen shed occurred earlier in the day (around 0800 – 0900 LST) when the morning winds were stronger during their two-year study. When the morning winds were lighter the peak pollen shed time was in the afternoon. Loubet et al. (2002) found that pollen emissions started when the air became drier in the morning around 0800 LST and lasted until 1500 LST. Vapor pressure deficit and canopy wetness were the variables that correlated best with pollen emissions (Loubet et al. 2002). Raynor et al. (1972) found more pollen grains were deposited next to the source

field than 60 m away from the source field; and that about twice as much of pollen fell inside the source field than outside it. The maximum deposition was at 1 m to 3 m from the source field (Loubet et al. 2002). Emberlin et al. (1999) found that 50% of the kernels of any individual plant results from pollen of plants within a 12 m radius.

There have been studies on the dispersion of glass beads (Wilson 2000) and seeds of trees (Nathan et al. 2002) that help to explain the pollen dispersion process. The glass beads used in Wilson's (2000) study were 50-100 μm, which is in the same range of sizes as pollen grains. The glass beads were released a few meters from the ground. Wilson (2000) then compared the deposition pattern to trajectory models. He found that with stable stratification had the narrowest deposition path and the unstable stratification had the widest deposition path. Since most of the pollen is released during dry, warm weather there will be thermals rising turbulently that will affect the pollen. The pollen can be brought upwards with velocities of 0.5 – 1.5 m s^{-1}. Once the pollen reaches higher elevations it can be transported horizontally farther than pollen that remained at the ground (Emberlin et al. 1999). Wilson (2000) also found that the leading edge of the deposition was located farther from the source field in unstable conditions than neutral conditions. In neutral conditions the pollen was located farther from the source field than in stable conditions.

Although the seeds of the trees used in Nathan et al. (2002) were slightly larger than the size of the pollen grains of maize, the study is useful since the seeds traveled long distances and most pollen studies did not include distances longer then 400 or 500 meters. Nathan et al. (2002) found the seeds of trees that were uplifted from the canopy would travel farther then those not uplifted. They used two flow regimes, one for short distance seed dispersal, controlled by within canopy flow, small wind speed, damped turbulence, and energetic eddies of approximately one-third the mean canopy height; and one for long distance seed dispersal, with a larger wind speed and eddy sizes that rapidly increase with height.

Wilson and Shaw (1977) list four ways vegetation interacts with and influences the wind flow in the lowest atmospheric layers:

1. "in extracting momentum from the flow due to the aerodynamic drag of the plant parts;
2. in converting kinetic energy of the mean flow into turbulent kinetic energy in the wakes formed behind obstructions to the flow;
3. in breaking down large-scale turbulent motions into smaller scale motions, again in the wake flow; and
4. in providing a buoyant contribution to the production of turbulent energy due to the convective transfer of sensible heat between the plant parts and the airstream."

The previous four effects are important in pollen dispersion. (1) The wind flow cannot go through a plant, therefore it must go around the plant parts, adjusting to the wind drag. This will cause the wind speed to decrease with depth in the vegetation. Figure 2.6 shows the Lagrangian pollen dispersion model's wind profile with maize at a height of 2 m and a wind speed of 2.635 m s^{-1} at a 2 m height (the height of the measurement). It is shown that the wind extrapolates to zero at the ground and has an exponential curve from the height of the canopy upwards. The log-wind profile (Equation 2.1) is used to take into the account of the wind drag from the plant canopy, shown as:

$$u(z) = \frac{u_*}{k} \ln\left(\frac{z - z_{pd}}{z_o}\right) \quad (2.1)$$

where u(z) is the wind at height z, u_* is the friction velocity, k is von Karman's constant = 0.4, z is height, z_{pd} is the zero-plane displacement, and z_o is the surface roughness length. The roughness length is defined as the height at which the neutral wind profile extrapolates to a zero wind speed (Oke 1979). The roughness length is a function of the shape and density of the roughness elements or canopy. (2) The kinetic energy of the mean flow gets converted to turbulent kinetic energy when the wind hits the maize canopy and the wind must find ways to go around the canopy parts (such as stems and leaves). (3) At the canopy the large scale turbulent motions will be broken up into smaller scale

turbulent motions because of the lack of open space in the canopy. When the wind comes in contact with the canopy the wind will form smaller scale turbulent motions to go around the canopy. (4) With eddies being formed from the plant canopy down to the ground sensible heat from the plant canopy will be transferred to the air with updrafts and downdrafts in the eddies.

All four of the effects to the wind flow are relevant to pollen dispersion since the pollen relies on the wind to move it from the tassel to the ear. When the wind flow changes direction due to the maize canopy and the turbulence that the canopy creates, the pollen will be dispersed in different directions. The turbulence will also create upward and downward moving eddies therefore allowing some of the pollen to be carried higher than the maize canopy and allowing the pollen to move further away from the canopy by the horizontal movements of the wind. Other pollen is brought down to the ground faster than if there is no wind.

Dispersion away from the source plots occurs not only by wind, but also by the carriage of bees (Emberlin et. al., 1999). The pollen dispersion model will not account for this type of dispersion because this is not a significant part in the dispersion of maize pollen.

2.3 Conclusion

In order for a maize plant to pollinate, pollen shed must overlap with silking. The pollen grains would have to fall straight down without being picked up by an updraft and without being carried away by wind. Maize often begins shedding pollen before the silks are receptive, resulting in 5% of a plant's kernels are pollinated from its own pollen grains (Emberlin et al. 1999). Outcross percentage of pollen grains in a field is important to know as mentioned in the introduction (chapter one).

Assuming an average wind speed of 2 m s^{-1} pollen can travel 14,400 m in two hours. In order for maize pollen to remain in the air for two hours it must be carried upward by turbulence. If

there are no updrafts the maize pollen will fall to the ground in ten seconds, in which case the pollen would travel twenty meters horizontally (in ten seconds).

Luna et al. (2001) found that the outcross percentage was 1% at 200 m. Assuming an average of 500 kernels / ear (Bassetti and Westgate, 1994), one ear / plant (National Corn Growers Association 2001), 30,000 plants / acre, 3000 pollen grains / silk (Westgate and Lizaso, unpublished), and 100 pollen grains / 20 viable pollen grains (Luna et al. 2001). The following equation shows how using the averages of a maize plant, 1% (equal to 1/100) outcross of pollen grains from a maize field is equal to 2.25×10^9 pollen grains/acre.

$$1\% = \frac{1}{100} * \frac{500\ \text{kernels}}{\text{ear}} * \frac{\text{ear}}{\text{plant}} * \frac{30{,}000\ \text{plants}}{\text{acre}} * \frac{\text{silk}}{\text{kernel}} * \frac{3000\ \text{grains}}{\text{silk}} * \frac{100\ \text{grains}}{20\ \text{viable grains}}$$

$$= 2.25 \times 10^9 \frac{\text{pollen grains}}{\text{acre}}.$$

It is important to note that there are many more pollen grains than there are silks on an ear of maize (3000 pollen grains / silk), meaning that not every pollen grain is needed to fertilize a kernel. Not every pollen grain will land on a silk and not every pollen grain that lands on a silk will pollinate the female flower (ovary). There is only one pollen grain that will pollinate a female flower. With a farm of 200 acres this means that there is a possibility of up to 4.5×10^{11} pollen grains from other fields. These pollen grains will also have to compete with the pollen grains released in that field to pollinate the female flower.

The previous example shows how much outcross there is 200 m from a source field, but most maize fields are placed closer than 200 m apart from each other. This would mean that there would be a higher percentage of outcross and more contaminated pollen grains per acre. The Lagrangian Pollen dispersion model will be used to predict where this outcross will occur and when coupled with a pollen viability model it can be used to predict the risk assessment of outcross in a maize field.

Figure 2.1. The parts of a maize plant, the tassel and anthers are located at the top part of the maize plant and the silk and ear are located in the middle of the maize plant.

Figure 2.2. A close-up view of the tassel and anthers of a maize plant.

Figure 2.3. A close-up view of the silk and ears of a maize plant.

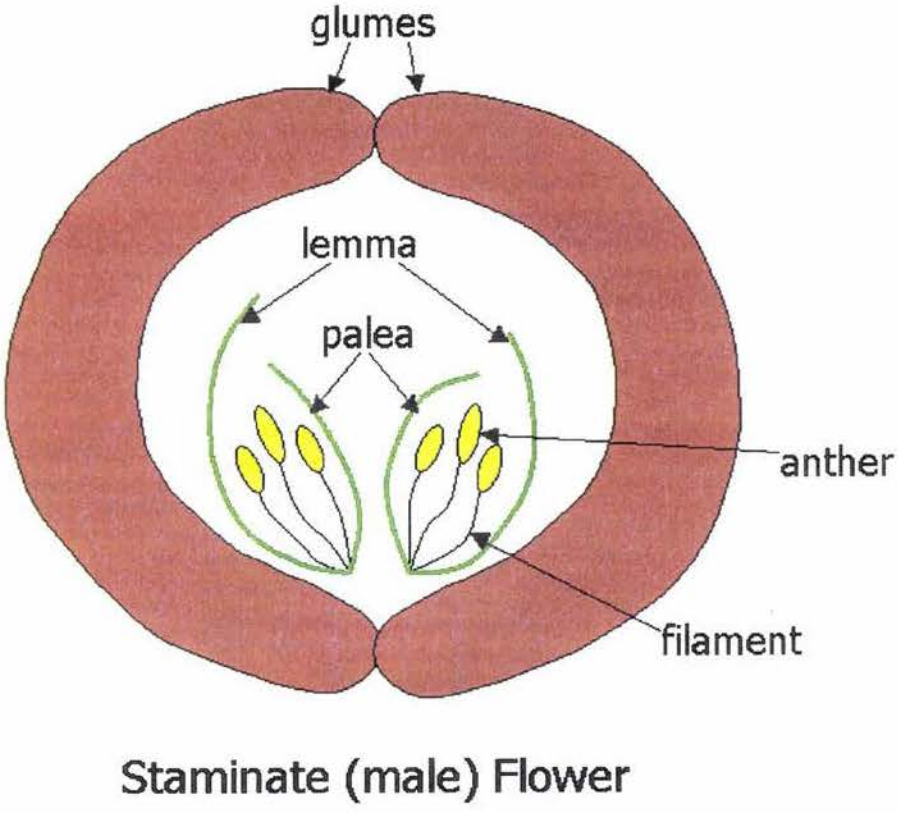

Figure 2.4. The Staminate (male) flower has two glumes, two lemmas and paleas, and two sets of three anthers and filaments.

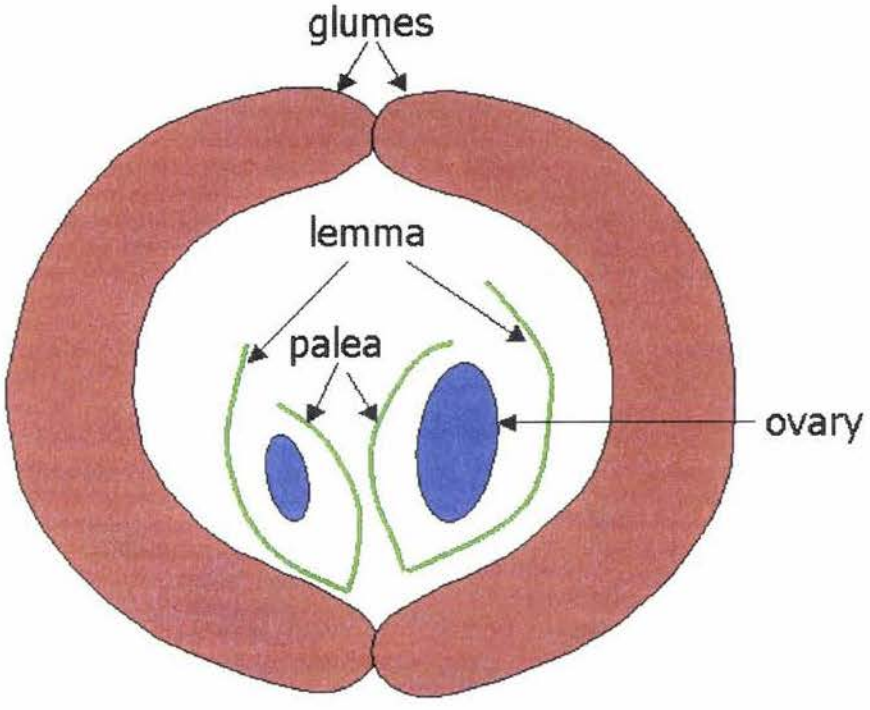

Pistillate (female) Flower

Figure 2.5. The Pistillate (female) flower has two glumes, two lemmas and paleas, and two ovaries; one of the ovaries is smaller and will eventually degenerate.

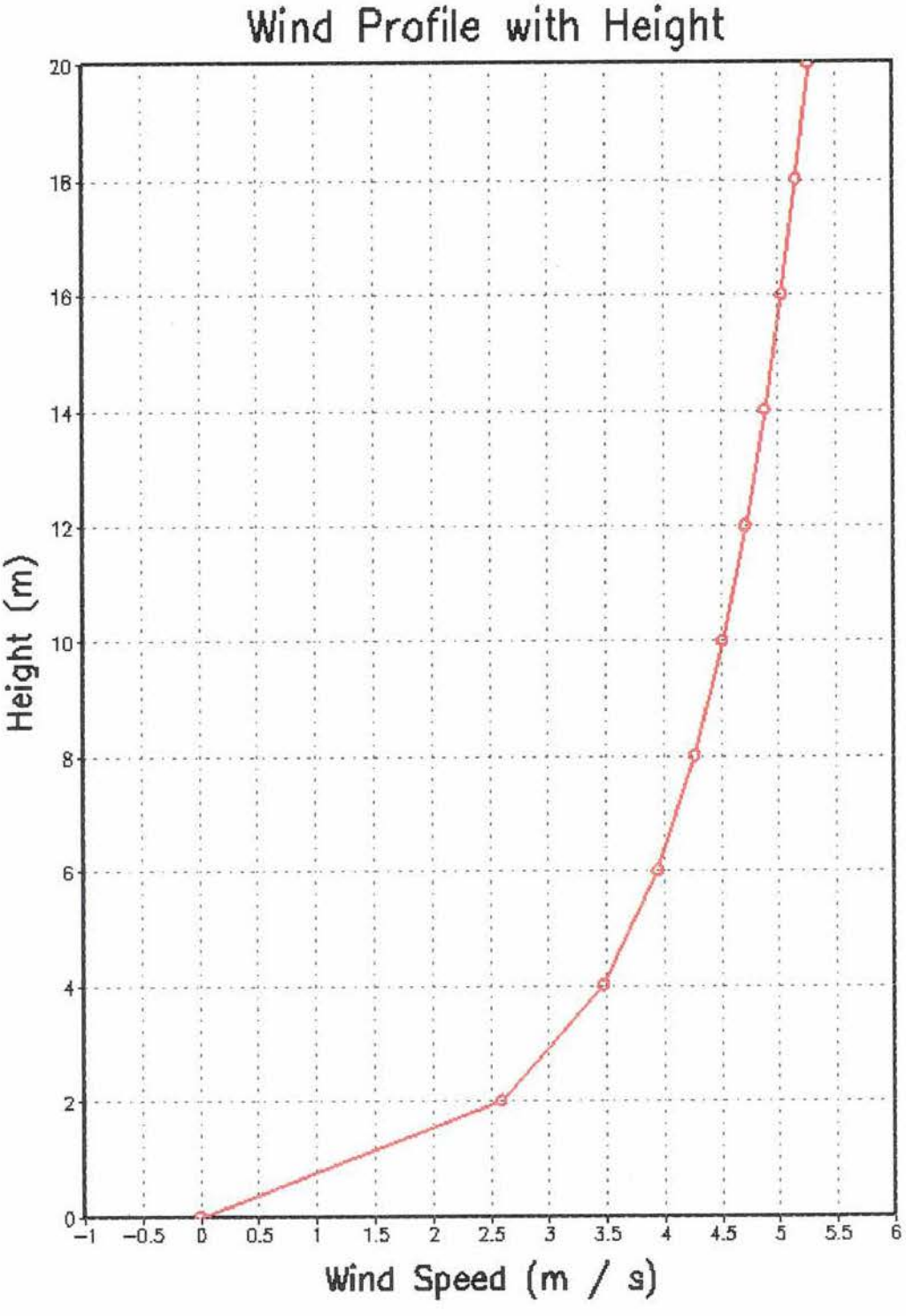

Figure 2.6. The wind profile with maize at a height of 2-meters and a wind speed of 2.63 at a height of 2-meters.

CHAPTER 3. BOUNDARY LAYER AND TURBULENCE

This chapter discusses the boundary-layer meteorology and turbulence effects in maize canopies. Boundary layer meteorology is important because it describes the layer of air just above the surface of the earth, which is where the pollen dispersion occurs. Turbulence is created from thermals rising from the ground or maize canopy and from wind coming in contact with the ground and maize canopy.

3.1 Boundary Layer Meteorology

Raupach et al. (1989, 1996) and Nathan (2002) say that a dispersion model should consist of two flows, one in the canopy with low velocities and one above the canopy with higher velocities. Raupach et al. (1989, 1996) found there is an inflection point with maximum velocity gradient at the tree top height. There can be constant turbulent fluxes with height if there are no sources and sinks above a canopy and the storage of heat in the air is neglected. Molder et al. (1999) found the underlying forest affects momentum exchange less than the heat and humidity exchange. Although trees are taller than maize plants, trees and maize plants have some similarities such as air (and wind) can pass though them (unlike a building) and they both have canopies. Research done on trees can compliment research on maize plants.

Cionco (1972) found that the wind speeds in the canopy are a function of height, canopy density, and element flexibility. Wind speed increases as canopy density and element flexibility increases. Immature maize is less dense but more flexible while mature maize is more dense and less flexible. Immature maize will have higher winds due to the greater flexibility and the shorter height of the canopy.

An exponential canopy wind profile is expected on the assumption of a height independent Prandtl mixing length (Wilson et al. 1982), used to relate shear stress to the mean velocity shear, and

a vertically uniform canopy. A sample wind profile used in the model is shown in Figure 2.6. The wind shear has a maximum at the height of the canopy top and within the canopy is almost exponential (Finnigan 2000). The rate of decrease is dependent on the attenuation coefficient, which uses wind flow and height of the canopy. Cionco (1972) found the attenuation coefficient to be 1.97 for a mature maize canopy.

A roughness sublayer is the region where the boundary layer is influenced by roughness elements at the ground (such as maize, forests, or buildings). A roughness sublayer height should be two times the height of the canopy (Raupach et al. 1996, Hogstrom et al. 1989, and Molder et al. 1999). Aylor and Flesch (2001) used a roughness sublayer equal to 1.3 times the height the canopy because of the relatively short and dense wheat and grass canopies used in their study. Molder et al. (1999) found above a forest stand, a roughness sublayer exists where eddy diffusivities are enhanced and gradients of meteorological variables are reduced; the extent of the roughness sublayer above the treetops can be several tree heights. Wake diffusion production enhances eddies just above the tree height but these eddies quickly dissipate. Mahrt (1997) says this roughness sublayer is shear dominated. The flow around the canopy is adjusted for up to 3 times the length of the canopy downstream (Coceal and Belcher 2003).

3.2 Turbulence

In the top two-thirds of the canopy the normalized standard deviations (or turbulent wind fluctuations) of u and v (σ_u and σ_v) increase with height. In the bottom third the values remain fairly constant. Turbulent intensity of the u, v, and w-components show a maximum at one-tenth the height of the canopy. For σ_v/σ_u a slight increase with the depth of the canopy is found. For σ_w/σ_u there is a maximum at 130 cm for mature maize. Shaw et al. (1974b) found $\sigma_u > \sigma_v > \sigma_w$ within and above the canopy where Wilson et al. (1982) found that σ_v grows larger than σ_u with depth of the canopy. Wilson et al. (1982) found that the vertical profiles of horizontal wind speeds $s(z)=(\sqrt{u^2+v^2})$ and $\bar{u}(z)$,

the standard deviations of the wind speeds (σ_u, σ_v, σ_w) and the momentum flux $\tau(z)$ can be normalized by their canopy top values to obtain profile shapes that vary little from day to day. The flow within the canopy may then be characterized by a single wind speed. All three components of relative intensity of turbulence (σ_u, σ_v, and σ_w) and the total relative intensity were higher within the maize canopy than above it and all increased with depth into the crop (Cionco, 1972). The model's σ_u, σ_v, and σ_w values are shown in Figure 3.1.

Shaw et al. (1974a) show the degree of correlation between the vertical and longitudinal components of the wind velocity is a function of height inside the crop. There is an increased correlation coefficient between u and w in the upper part of the canopy. They also found the same to be true for temperature and vertical velocity.

The non-dimensional wind profile (ϕ_m) is given by (Hogstrom 1996):

$$\frac{\partial u}{\partial z}\frac{kz}{u_*} = \phi_m\left(\frac{z}{L}\right) \quad (3.1)$$

where u is the magnitude of the horizontal wind vector and L is the Obukhov length (is the height above the surface where buoyant factors first dominate over mechanical or shear turbulence). The non-dimensional wind profile (ϕ_m) is a function of L, which is representative of stability. In the neutral boundary layer vertical motion is formed in the lowest layers of the air from forced convection due to frictionally generated eddies (Oke 1979). In neutral conditions the up and down drafts come from forced convection fluctuations. In the near-neutral boundary layer, the transport of pollen may occur as a sequence of several smaller scale shear-dominated eddies where the pollen will be transported through the boundary layer from many individual eddies at different levels (Mahrt 1997).

For strong instability, or local free convection, buoyancy dominates the local turbulence production process and so ϕ_m is proportional to negative z/L with an exponent given by classical

dimensional analysis of −1/3 (Hogstrom 1996). For unstable stratification the model uses the following:

$$\sigma_w = 1.25u_*(1-3\frac{z}{L})^{1/3} \quad (3.2)$$

from Garratt (1992).

The turbulent transport (which describes how turbulent kinetic energy is moved around by turbulent eddies) and pressure transport (which describes how turbulent kinetic energy is moved around by pressure perturbations such as buoyancy) terms in the turbulent kinetic energy equation become more important in the unstable case; they have opposite signs and are approximately the same magnitude (Hogstrom 1996). This causes the vertical movement of eddies (and therefore momentum flux) to be enhanced. Near the surface mechanical effects continue to dominate but at greater heights thermal effects become increasingly important (Oke 1979). Strong instability weakens the wind gradient by promoting vertical exchange over a deep layer, and thereby mixing the greater momentum of faster moving upper air with that nearer the surface (Oke 1979). This is important to the pollen model since the vertical movement of eddies affect pollen grain movement. When the eddies move upward, the pollen grains will also move up, this means the pollen grains will be entering areas of greater wind speeds and can travel farther from the source field. When the eddies move downward, the pollen grains will also move down, this means the pollen grains will be entering areas of decreased wind speeds and will land closer to the source field than if the eddies did not bring them closer to the ground or plant.

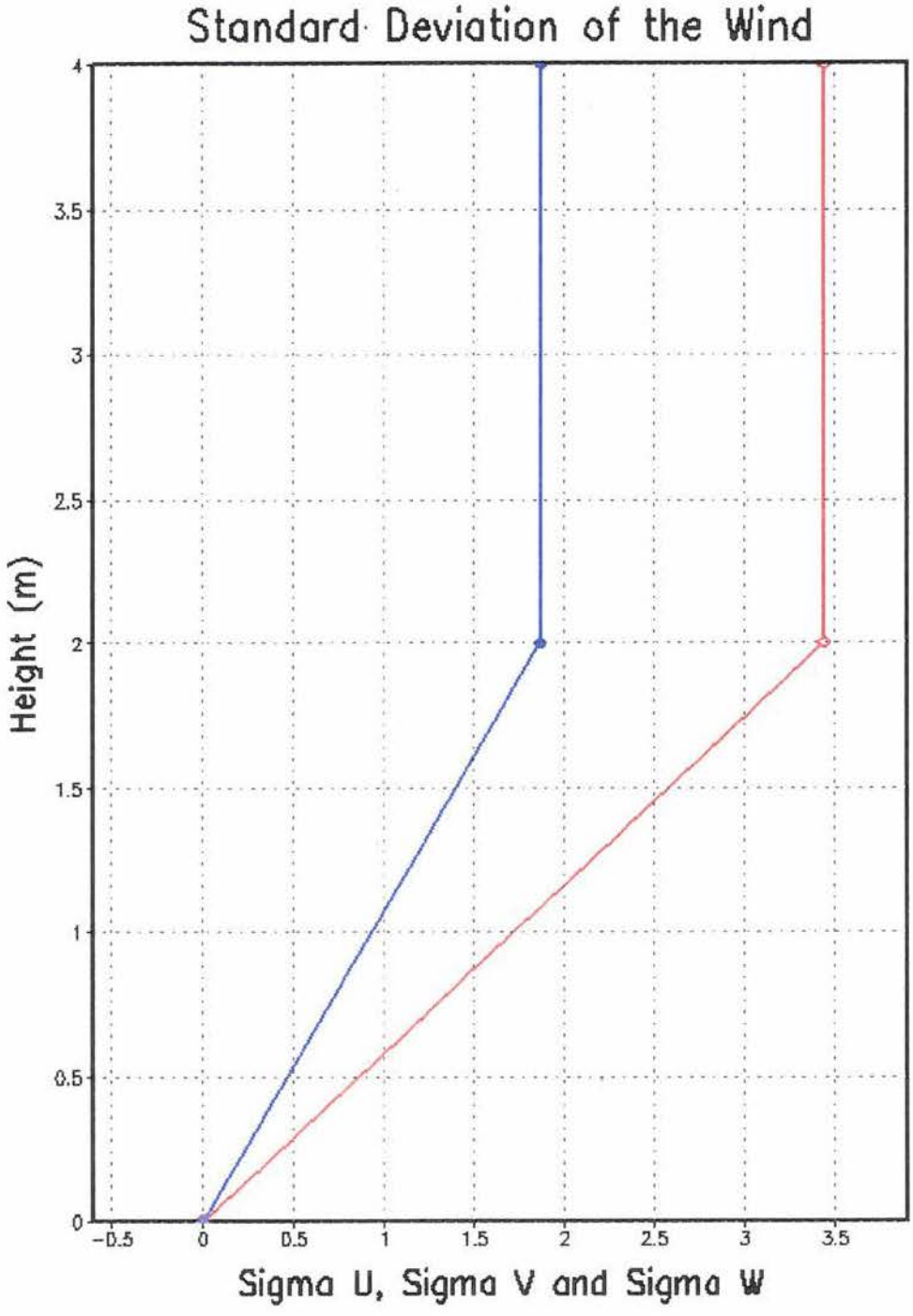

Figure 3.1. The σ_u (red), σ_v (red), and σ_w (blue) values in the pollen dispersion model. The model set $\sigma_u = \sigma_v$.

CHAPTER 4. THE POLLEN DISPERSION MODEL

4.1 The Lagrangian Pollen Dispersion Model as a Model in a Model

The Lagrangian pollen dispersion model is a sub-model in a group of sub-models used for pollen risk assessment as shown in Figure 4.1. Each of the models does one task to assess risk of pollen outcross. The meteorological analysis is a physical model that evaluates the atmospheric conditions from before pollen shed to pollination. The pollen shed model is a biological model that predicts the timing and amount of pollen shed. The Lagrangian pollen dispersion model is a physical model that predicts the movement of the pollen from the tassel to its landing spot. The receptor model predicts the amount of pollen that will land on maize silk. The pollen viability model is a biological model that predicts the viability of pollen that lands on maize silk. And the risk assessment model predicts the amount of outcross a maize field has.

Since each model performs one task, that sub-model can be developed without the other sub-models. Another benefit of developing sub-models is that two or more sub-models can be developed at the same time and all the sub-models can be used independent of each other. The models will interactively work together to form a coupled physical and biological pollen risk assessment model. This study is on the pollen dispersion model.

4.2 Why Make a Lagrangian Model?

This model is based on the approach from the Lagrangian Particle Dispersion model in McNider (1981). The model is Lagrangian because the calculations are on the moving particles (or pollen grains) rather than on a fixed grid in the model. A Lagrangian model is very costly in computer time when a large number of particles are used since the model has to keep track of individual pollen grains and do calculations (velocity, fall speed, etc.) on each pollen grain rather than on a grid scale at each time step (McNider 1981).

Although the Lagrangian pollen dispersion model is costly in computer time, it is useful to know what source each pollen grain originated from and what path it took to the ground. This is especially useful for combining the model with the other sub-models, such as the pollen viability model, since that model needs to known how long the pollen grains were in the air and what the atmospheric conditions were while the pollen was in the air.

Each pollen grain moves according to the mean and turbulent wind at its location. For each time step the following calculations are made on each pollen grain:

$$x(t + \Delta t) = x(t) + \Delta t[\bar{u}\ (t) + u'(t)] \qquad (4.1)$$

$$y(t + \Delta t) = y(t) + \Delta t[\bar{v}\ (t) + v'(t)] \qquad (4.2)$$

$$z(t + \Delta t) = z(t) + \Delta t[\bar{w}\ (t) + w'(t)] \qquad (4.3)$$

where the overbars stand for mean wind and the primes for turbulent wind. These equations show that the pollen grains move from their current location at x, y, and z at time t to a new position at time Δt according to the mean wind speed and turbulent wind speed at time t. The turbulent wind speed is determined from turbulence, particle position, time step, and a random number. The equations used in the model are:

$$u' = e^{R(\Delta t)} * u' + \sqrt{1 - (e^{R(\Delta t)})^2} * \sigma_u * ran \qquad (4.4)$$

$$v' = e^{R(\Delta t)} * v' + \sqrt{1 - (e^{R(\Delta t)})^2} * \sigma_v * ran \qquad (4.5)$$

$$w' = e^{R(\Delta t)} * w' + \sqrt{1 - (e^{R(\Delta t)})^2} * \sigma_w * ran \qquad (4.6)$$

$$R(\Delta t) = e^{-\Delta t / T_L} \qquad (4.7)$$

where ran is a random number generated in the model and T_L is the Lagrangian timescale described later. The random number is generated from a random number generator using a mean of 0.0 and standard deviation of 1.0. This random number allows the particle motions to fluctuate with time.

4.3 Lagrangian Pollen Dispersion Model

The pollen dispersion model uses a zero-plane displacement, such that logarithmic wind speed with height starts at the zero-plane displacement height, d. For the pollen dispersion model d equals 0.5 m. Garratt (1992) says that there is a breakdown of the inertial sublayer profile at low z/z_o values even with a zero-plane displacement.

For the turbulent wind speeds of u and v in the unstable atmosphere ($h/L < 0$) and the stable and neutral atmosphere ($h/L \geq 0$) the Lagrangian pollen dispersion model uses:

$$\sigma_u = \sigma_v = u_*(12 - 0.5\frac{h}{L})^{1/3} \quad \text{for } h/L < 0 \qquad (4.8)$$

$$\sigma_u = \sigma_v = 2.29u_* \quad \text{for } h/L \geq 0 \qquad (4.9)$$

from Garratt (1992) where σ_u and σ_v are the standard deviation of the horizontal wind speed in the x and y direction, u_* is the friction velocity, h is the planetary boundary layer height, and L is the Obukhov length. The Obukhov length is proportional to the height at which buoyant factors first dominate over mechanical (shear) production of turbulence (Stull 1988). The σ_u and σ_v values remain constant because the model has steady state conditions for friction velocity and the standard deviations of the wind above the corn canopy (two meters).

If a time step is larger then the Lagrangian timescale, the particle loses its memory of the previous turbulent velocity and moves fully randomly (Uliasz 1993). A time step of 0.5 s is used in the model. The Lagrangian timescale (from Wilson 2000) in the model is:

$$T_L = \frac{\alpha z}{\sigma_w} \qquad (4.10)$$

where T_L is the Lagrangian timescale, α is a coefficient equal to 0.5, z is the height of the particle, and σ_w is the standard deviation of the vertical velocity (turbulent velocity) of the particle.

Sensible heat flux is used in the pollen dispersion model to indicate atmospheric stability. When the sensible heat flux is 0 W m^{-2}, the atmospheric stability is neutral. During the time of day

when pollen dispersion takes place (the morning to early afternoon) the atmosphere is generally unstable. When the atmosphere is unstable is put into the model the pollen grains should travel farther from the source field than under neutral conditions. This is because of the mixing in the air caused by instability and the mixing can carry the pollen grains farther downwind than neutral conditions. The Obukhov length is proportional to the height where buoyant factors first dominate over shear production of turbulence (Stull 1988). Sensible heat flux is used to compute the Obukhov length, as given in the following equation:

$$L = \frac{\rho c_p T_{ref} u_*^3}{kgH} \qquad (4.11)$$

where ρ is density, c_p is the specific heat for dry air (1004 J kg^{-1} K^{-1}), T_{ref} is the reference temperature, u_* is the friction velocity, k is the von Karman constant (0.4), g is gravity, and H is sensible heat flux.

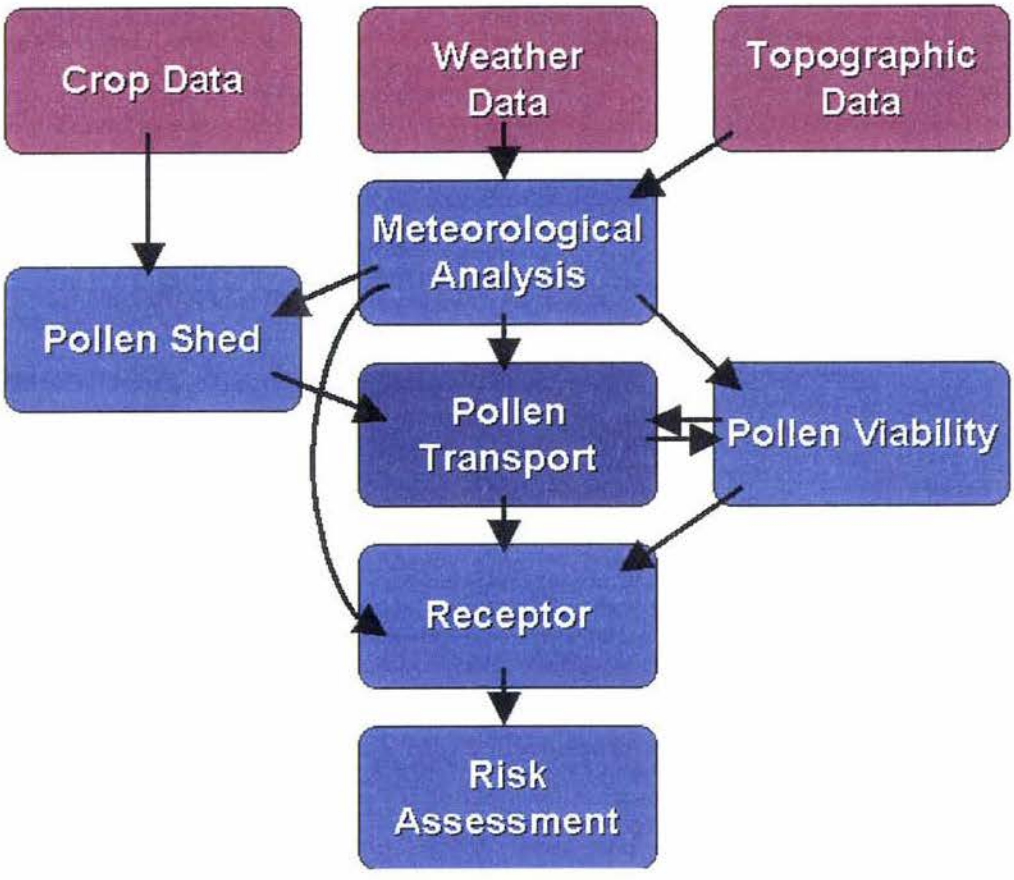

Figure 4.1. A diagram of submodels (shown in blue) and input data (shown in red) of the complete pollen risk assessment model. The pollen transport submodel is the model discussed in this study.

CHAPTER 5. MODEL VERIFICATION

5.1 Introduction to the Verification

The Lagrangian model is compared with field observations and a Gaussian model to see how accurately the model predicts the dispersion of pollen grains. To compare the models pollen count data was obtained from Mark Westgate and Dale Ireland from July 21, 23, 24, and 27, 2000. The source field was located near the Ames, IA municipal airport and was 50 feet wide by 100 feet long. There were three maize fields surrounding the source field at 1300 feet to the south, 1200 feet to the north, and 800 feet to the east-northeast (Ashton et al. 2000). Pollen counts were collected at 5, 10, 30, 90, 165, and 330 feet from the source field in the north, northeast, east, southeast, south, southwest, west, and northwest directions, along with nine equally spaced receptors inside the source field. Figure 5.1 shows the location of the receptors used in the field observations.

The Lagrangian model uses 81 sources to make up the source field. There are 9 sources in each row and column that are equally spaced apart from each other. Some model runs were completed with variable pollen dispersion from each receptor based on the percentage of pollen grain counts in each section of the source field from observations. The results showed that this could not be used because pollen grains from one section of the source field enter the adjoining sections of the source field. This caused the source field concentrations to increase in the sections downwind of the other sections. The results did not conform to the observations in the source field by this method. Observations would have to be taken to find out the pollen shed rate for each section of the source field. Therefore each source in all the model runs was specified to have an equal number of pollen grains coming from it (equal to one pollen grain per time step for the first fifty minutes of the model run).

The Lagrangian pollen dispersion model also computed pollen dispersion with a parametric estimator, which uses a Gaussian distribution, to estimate the amount of pollen grains that will fall in

each grid box. The parametric estimator allows fewer pollen grains to be released from the model by smoothing the deposition using a normal distribution. The parametric output was also compared with the observations and Gaussian model.

The pollen dispersion model was compared to a Gaussian model called the Industrial Source Complex Short Term, version 3 (ISCST3). The ISCST3 model's primary use is in industrial situations to predict air quality for distances less then 50 km (Ashton et al. 2000). It is useful to see if the models are comparable to each other since the Gaussian model has been used before in pollen dispersion and many air pollution studies. If the two models have large differences in pollen dispersion there will be a need for more work done to see why the two models differ.

There are some problems when comparing the pollen dispersion model with observations. The first problem is that the model has a grid spacing of 2 meters squared and the observations were given in centimeter squared values. This means the model data at 2 meters is a factor of 2×10^4 times greater then the observational data. The second problem is the model released 486,000 pollen grains and on average when maize is releasing pollen it sheds on average 1500 grains per square centimeter per day (Ashton et al. 2000), which equates to 2.787×10^{10} pollen grains from the source field. This means that the observations have 5.73×10^4 more pollen grains than the model.

Since both of these problems will greatly affect the values of the observation data and model data, the comparisons will not be made with value for value actual pollen amounts. The comparisons were made by converting the model pollen grain deposition from m^2 to cm^2 values then using a scaling factor that relates the total model pollen grains to observed pollen grains at the receptors.

The verification used ten individual model runs for each day. Each model run uses the average sensible heat flux, wind speed, and direction for that hour. These ten runs are one hour long for each of the ten hours that pollen released. The pollen grains are released for the first fifty minutes of each model run, allowing ten minutes for the pollen grains to land on the ground or go out of the model domain. The ten runs are multiplied by the percentage of the diurnal pollen shed shown in

Figure 5.2. The graph assumes the estimated pollen shed occurs for ten hours (8:00 local time to 17:00 local time) and the peak emission occurs at 11:00 local time (Westgate, unpublished). In reality the curve changes daily based on the humidity, wind speed, and temperature. For instance pollen shed does not occur when humidity is greater than 90%. Data were not available to include these changes in the model.

5.2 Comparison with Observations and a Gaussian Model

The wind roses for July 21, 23, 24, and 27, 2000 are shown in Figures 5.3, 5.6, 5.9, and 5.12 respectively. On July 21 and 24, 2000 there was not a lot of variability in the wind. The average wind speed for July 21, 2000 from 8:00 local time to 17:00 local time was 2.6 m s^{-1} and the average wind direction was 337°. The average wind speed for July 24, 2000 from 8:00 local time to 17:00 local time was 2.8 m s^{-1} and the average wind direction was 166°. Figure 5.4 shows the observations, Lagrangian model runs, and Gaussian model run for July 21, 2000. Figure 5.10 shows the observations, Lagrangian model runs, and Gaussian model run for July 24, 2000. The observations for July 24, 2000 show pollen grains in a small section southeast of the source field. On both days the Lagrangian pollen dispersion and the ISCST3 models predicted the pollen to fall in the same directions as the wind, which is expected.

On July 24, 2000 the observations could differ from the models because of the density of pollen receptors. For the field observations to contour from the northwest section of the source field there would have to be pollen grains falling on the northwest axes of the source field. The model has grid boxes between the north and northwest axes and therefore can deposit the pollen between the two axes. Both the Lagrangian pollen dispersion model and ISCST3 models represented the deposition of pollen grains well in the north direction and poorly in the northwest and southeast directions compared to the observations. The observations show pollen dispersion on the northwest axes where the models do not. This could have come from wind directions changing to the northwest and back to

the north between the fifteen-minute weather observations that the models have as input. On this day the Lagrangian model has the pollen being deposited the farthest from the source field, because this day had the highest wind speeds.

There was a lot of variability in wind speed and direction for July 23 and 27, 2000 from 8:00 local time to 17:00 local time as shown in Figures 5.6 and 5.12 respectively. As mentioned earlier there were ten model runs completed for each verification day. Each of the ten model runs used an average wind speed and direction for one hour of observations to account for the day's variability in wind speed and direction. Figures 5.7 and 5.13 show the observations, Lagrangian model runs, and Gaussian model run for July 23 and 27, 2000 respectively. The observations for July 23, 2000 show pollen grains on the far east and west locations of the domain along with the a small section southeast of the source field. The observations for July 27, 2000 show pollen grains on the far north and east locations of the domain along with a small section southeast of the source field. The observations from the north, east, and west could have been pollen grains from maize fields located around the source field or from small meteorological features that would not be picked up from weather observations every fifteen minutes. One possible reason for the small section southeast of the source field could be small scale turbulence that did not show up in the weather observations.

On July 27, 2000 the Lagrangian pollen dispersion model does not have the pollen dispersing far from the source field, due to the low wind speeds that occurred (Figure 5.13). With low wind speeds, the pollen will not travel far from the source field. The ISCST3 model has pollen traveling to the south out of the source field. This might be from inputting wind speeds every fifteen minutes instead of averaging the wind speeds for an hour like the Lagrangian pollen dispersion model. The observations show pollen in the far north, northeast, and east directions from the source field. These observations could have been pollen from other fields located around the source field.

Both the Lagrangian pollen dispersion model and ISCST3 models were able to represent the deposition of pollen grains well. Figures 5.5, 5.8, 5.11, and 5.14 show the deposition profile over all

the axes of the pollen grains for each model and the observations for July 21, 23, 24, and 27, 2000 respectively. Both models decrease the amount of pollen grains with distance from the source field, as expected. On July 23 and 27, 2000 the observations show an increase at 330 ft. This could be contamination from fields around the source field or small meteorological conditions not picked up in the fifteen minute data observations. On July 24, 2000 the ISCST3 model does a good job of matching up with the observations at the farthest distances (330 ft and 660 ft), when the Lagrangian pollen dispersion model does not have any pollen traveling that far. In general the ISCST3 did a better job at matching up with the observations at farther distances (90 ft to 660 ft) than the Lagrangian model; and the Lagrangian model did a better job at matching up with the observations at closer distances (5 ft to 30 ft) than the ISCST3.

The R^2 values between the two models and the observations and between the Lagrangian model and the ISCST3 model for downwind of the source field are shown in Table 5.1. These values are significant at the 99% level. The values are only shown for downwind of the source field because that is where most of the pollen grains (outside the source field and farther from the source field) are deposited and hence the most important directions. These value show how much of the variability is explained in the model. A value of 1.0 would show that the model has a perfect linear relationship with observations. A value of 0.774 (July 21, 2000 raw concentrations) says that the model explains 77.4% of the variance in the observations.

On July 27, 2000 the correlations are low. This could be from low wind speeds and amount of variability in the wind direction from that day. The Lagrangian pollen dispersion model assumes the wind speed and direction to be constant for an entire hour, so gusts and high wind speeds from July 27, 2000 would not be used in the model to push the pollen grains travel farther from the source field and the amount of variability in the wind direction is averaged out. A limitation of the model is that it does not allow for varying wind speeds and directions within each of simulation. Even if the

model did allow for varying wind speeds and directions the observations were given in fifteen minute time steps and they do not include wind gusts.

Tables 5.2, 5.3, 5.4, and 5.5 show the percentages for the pollen grains deposited in the source field for July 21, 23, 24, and 27, 2000 respectively. It is shown here that the Lagrangian particle dispersion model's raw concentrations matched up (or tied for) the best with the observations on all four days. Although the ISCST3 model run's were set to a 75% deposition in the source field, more pollen grains could have landed on the nine receptors in the source field than other locations in the source field.

5.3 Results

After comparing the Lagrangian pollen dispersion model with observations and a Gaussian model it was found that the Lagrangian pollen dispersion model matched up well with the observations and Gaussian model. Both models deposited the pollen grains downwind of the source field and decreased the amount of the pollen grains deposited with distance away from the source field, as expected from the observations. The Lagrangian pollen dispersion model had source field deposition percentage of pollen grains closer to the observations than the Gaussian model. On all the low wind variability days (July 21 and 24, 2000) the downwind axes had higher correlations with the observations for the Lagrangian model than the Guassian model. On the two days with variable wind speeds and directions (July 23 and 27, 2000) the Gaussian model had higher correlations with the observations than the Lagrangian pollen dispersion model. This could be because the Gaussian model allowed for more variability of the wind speed and direction, with fifteen minute observations, than the Lagrangian pollen dispersion model, with averaged hourly observations.

Overall, both the Lagrangian pollen dispersion model and Gaussian model had results that showed it is possible to model pollen dispersion. The models can give estimates on what the expected pollen dispersion deposition will look like.

Table 5.1. R^2 values for the Lagrangian and ISCST3 models versus the observations and the ISCST3 model versus the Lagrangian model for the downwind axes of each day. All values are significant at the 99% level, except where noted.

	Lagrangian		ISCST3	ISCST3 vs Lagrangian	
	raw	parametric		raw	parametric
July 21, 2000	0.774	0.772	0.223*	0.485	0.562
July 23, 2000	0.652	0.795	0.851	0.687	0.968
July 24, 2000	0.804	0.800	0.864	0.804	0.800
July 27, 2000	0.210	0.273	0.428	0.210	0.273

* Significant at the 95% level.

Table 5.2. The percentage of pollen grains deposited in the source field for July 21, 2000.

	% of pollen grains in the source field
Observations	92%
Raw	89%
Parametric	87%
ISCST3	89%

Table 5.3. The percentage of pollen grains deposited in the source field for July 23, 2000.

	% of pollen grains in the source field
Observations	96%
Raw	91%
Parametric	89%
ISCST3	87%

Table 5.4. The percentage of pollen grains deposited in the source field for July 24, 2000.

	% of pollen grains in the source field
Observations	98%
Raw	92%
Parametric	90%
ISCST3	88%

Table 5.5. The percentage of pollen grains deposited in the source field for July 27, 2000.

	% of pollen grains in the source field
Observations	98%
Raw	92%
Parametric	90%
ISCST3	87%

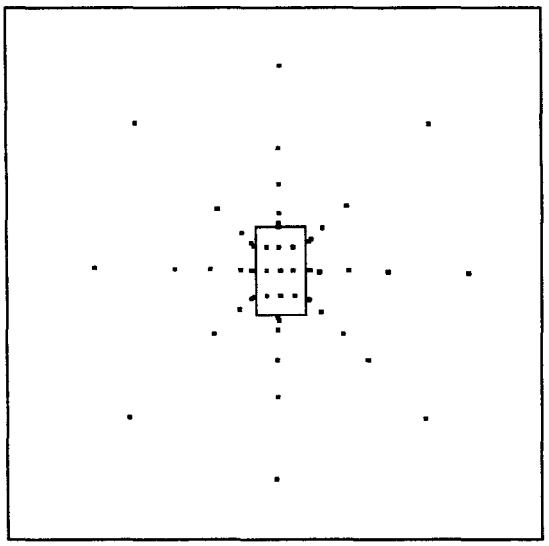

Figure 5.1. The location of all of the receptors during the July 2000 field experiment. The rectangle indicates the source field (Ashton et al. 2000).

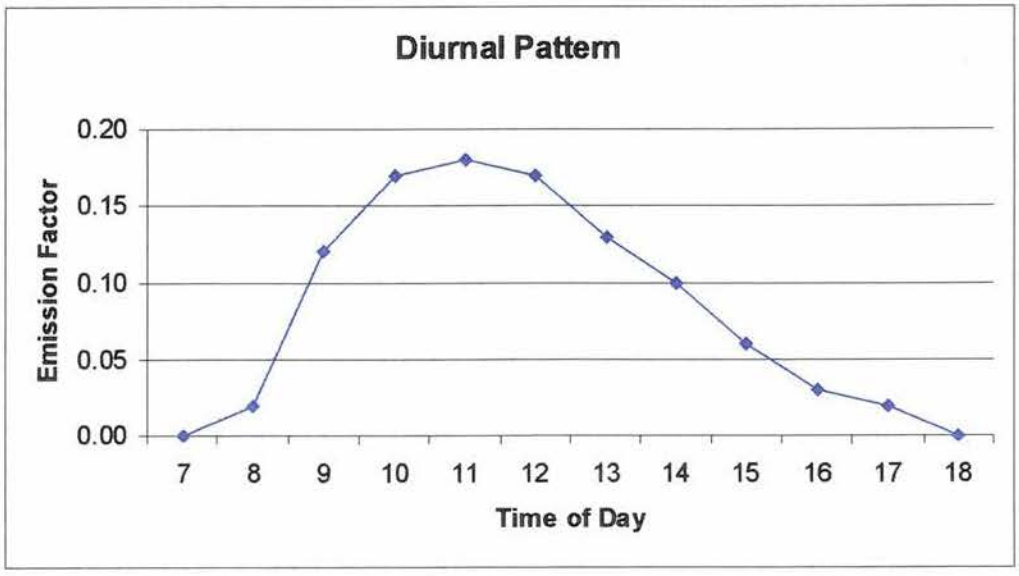

Figure 5.2. The diurnal pollen shed pattern (Westgate, unpublished).

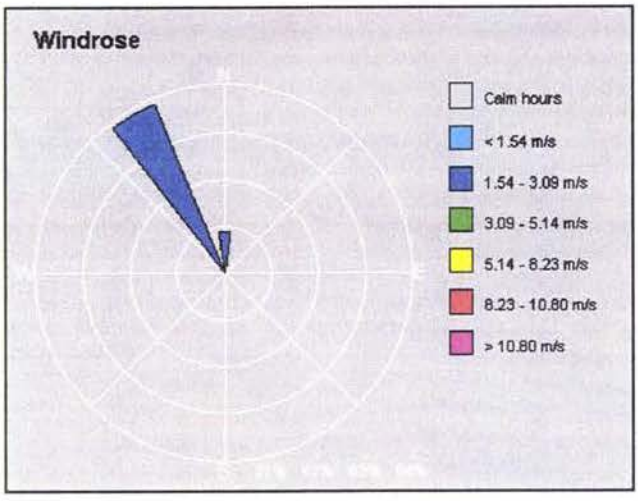

Figure 5.3. The wind rose from July 21, 2000 (Ashton et al. 2000).

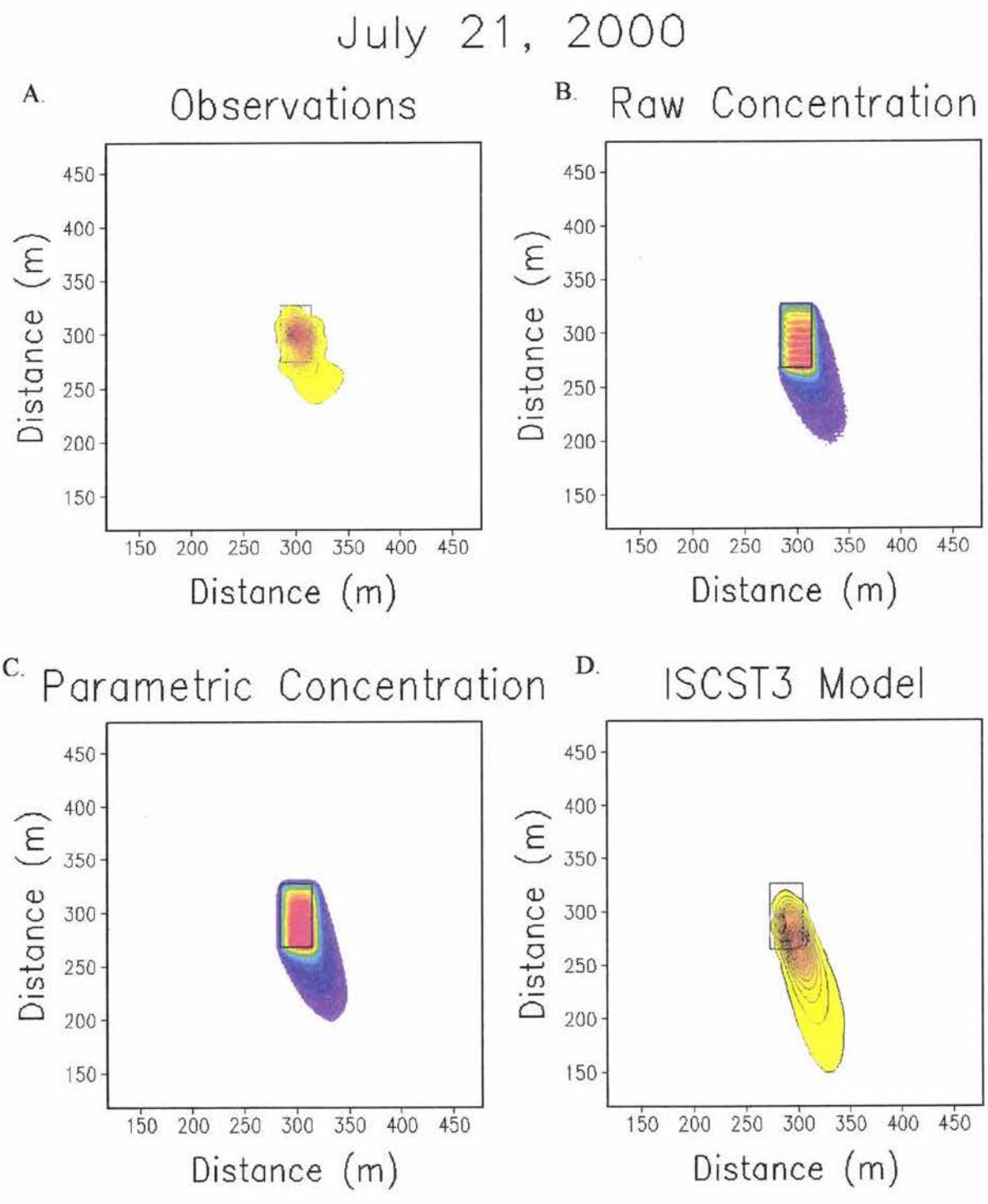

Figure 5.4. (A) Observed pollen counts (Ashton et al. 2000), the Lagrangian pollen dispersion model's predicted (B) raw concentrations and (C) parametric concentrations, and the (D) ISCST3's (Ashton et al. 2000) predicted concentrations for July 21, 2000. The rectangle is the source field.

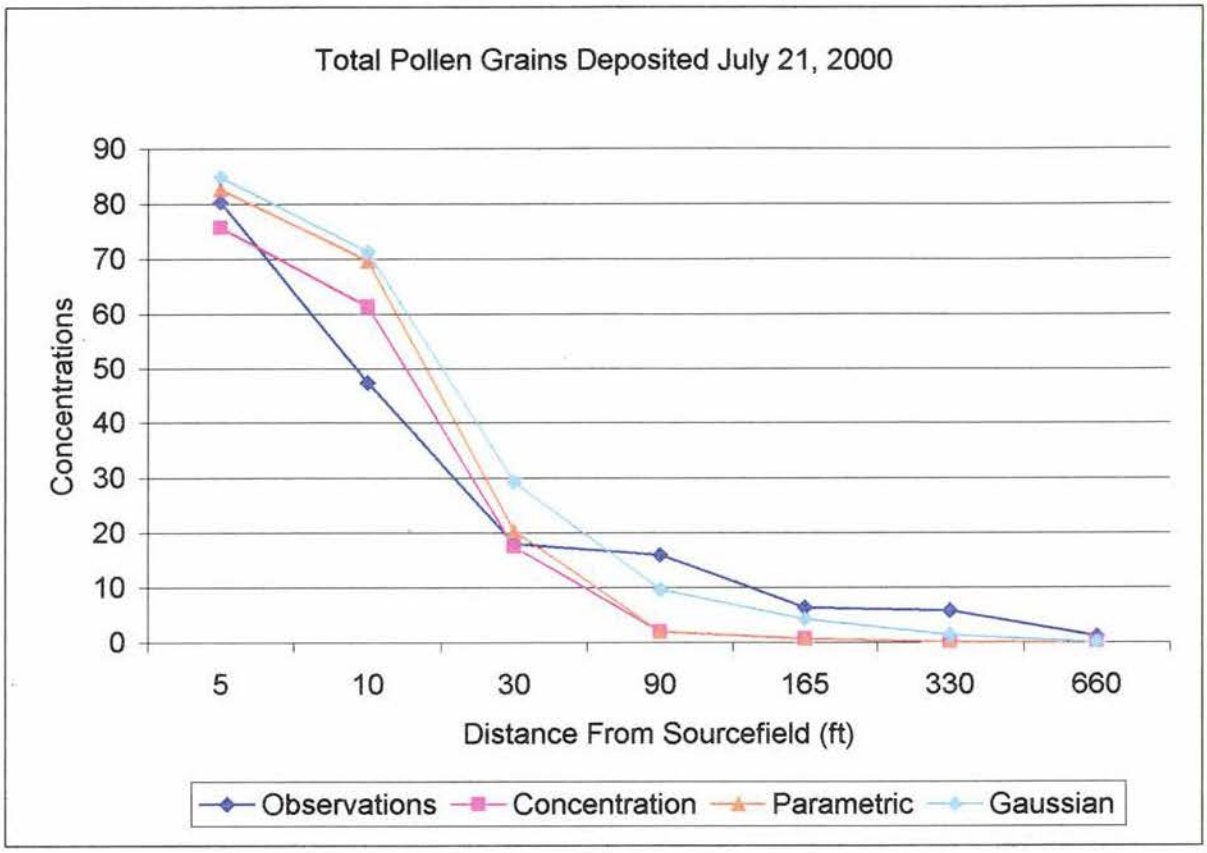

Figure 5.5. The July 21, 2000 deposition profile of all the axes over the distance away from the source field. The deposition is given in grains cm^{-2}.

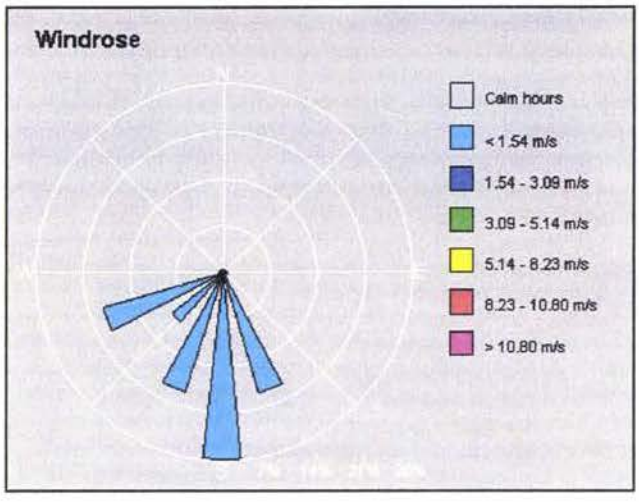

Figure 5.6. The wind rose from July 23, 2000 (Ashton et al. 2000).

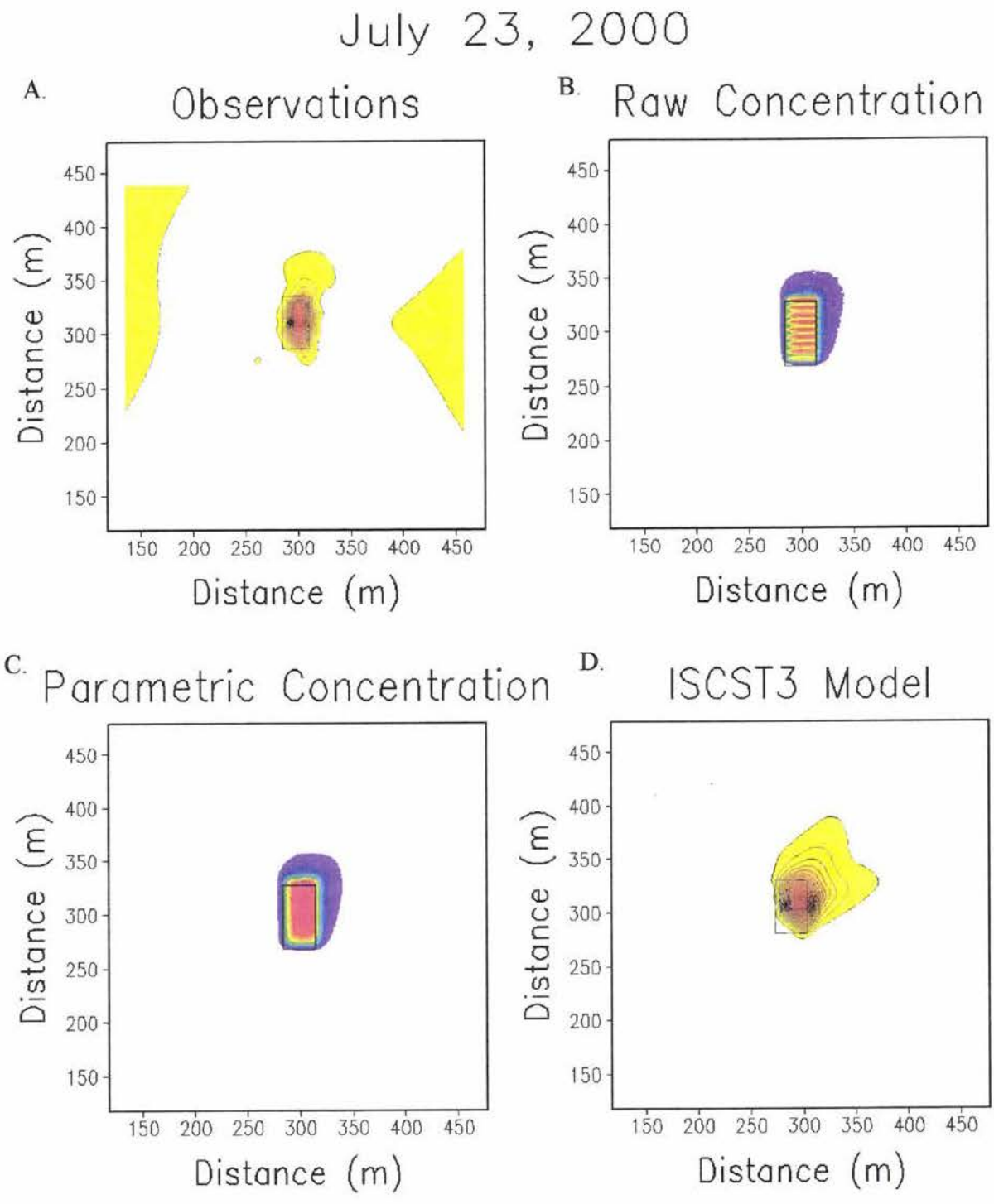

Figure 5.7. (A) Observed pollen counts (Ashton et al. 2000), the Lagrangian pollen dispersion model's predicted (B) raw concentrations and (C) parametric concentrations, and the (D) ISCST3's (Ashton et al. 2000) predicted concentrations for July 23, 2000. The rectangle is the source field.

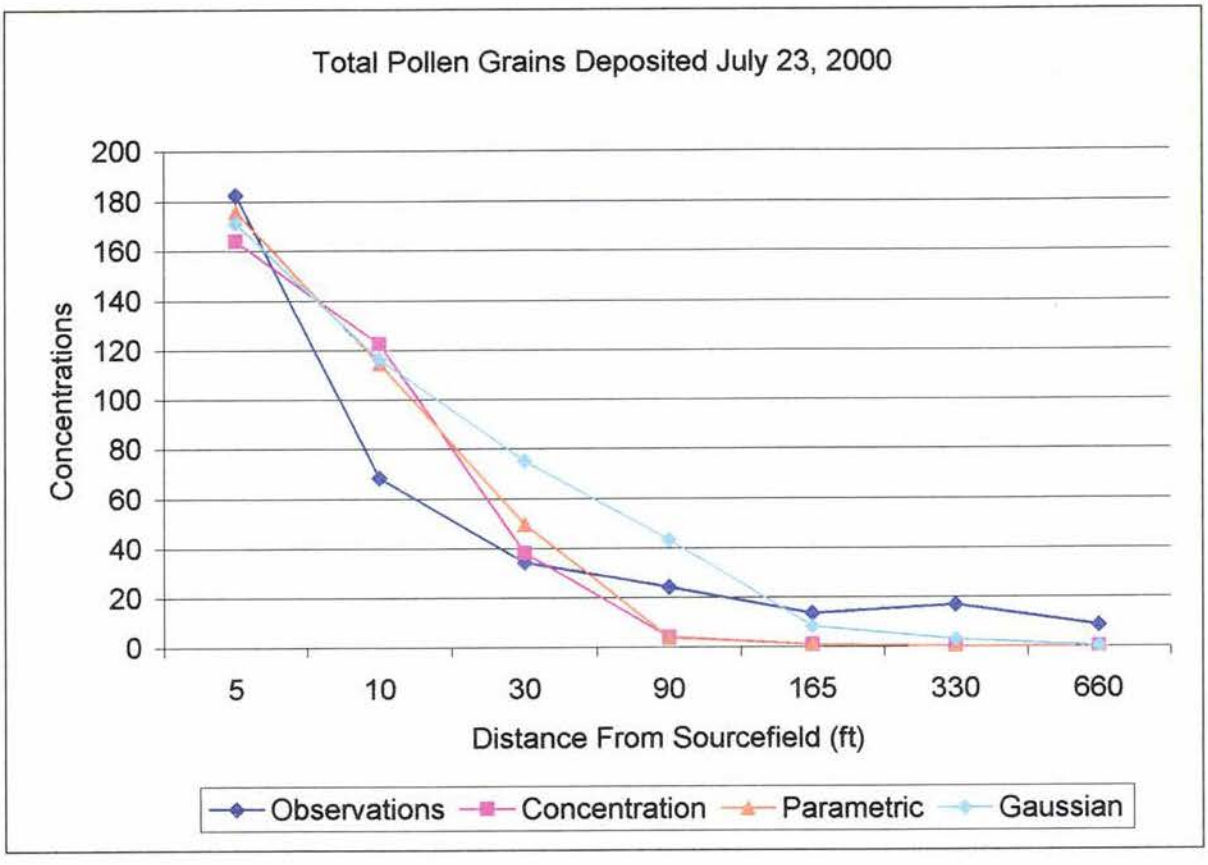

Figure 5.8. The July 23, 2000 deposition profile of all the axes over the distance away from the source field. The deposition is given in grains cm^{-2}.

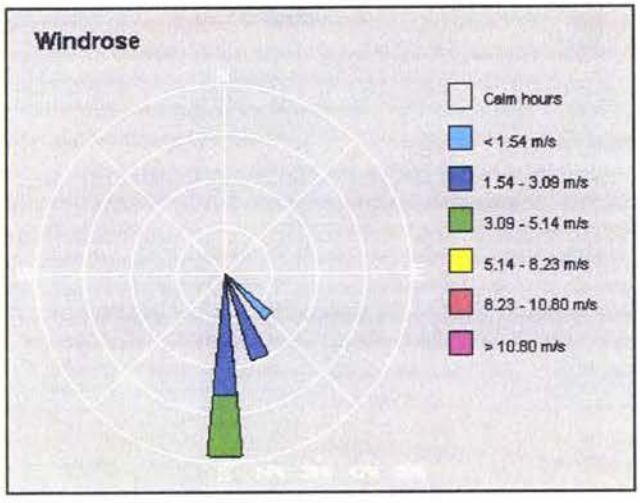

Figure. 5.9. The wind rose for July 24, 2000 (Ashton et al. 2000).

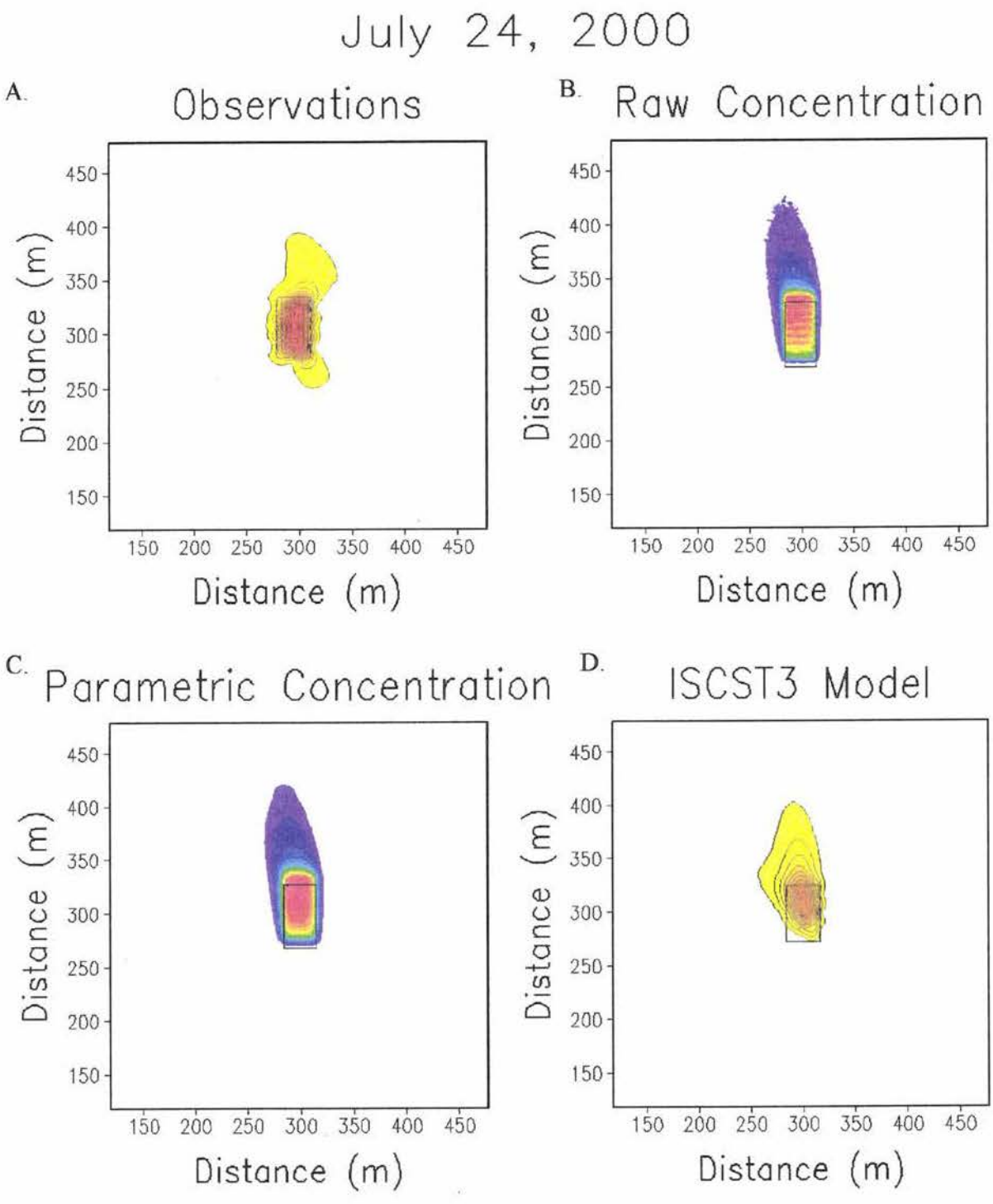

Figure 5.10. (A) Observed pollen counts (Ashton et al. 2000), the Lagrangian pollen dispersion model's predicted (B) raw concentrations and (C) parametric concentrations, and the (D) ISCST3's (Ashton et al. 2000) predicted concentrations for July 24, 2000. The rectangle is the source field.

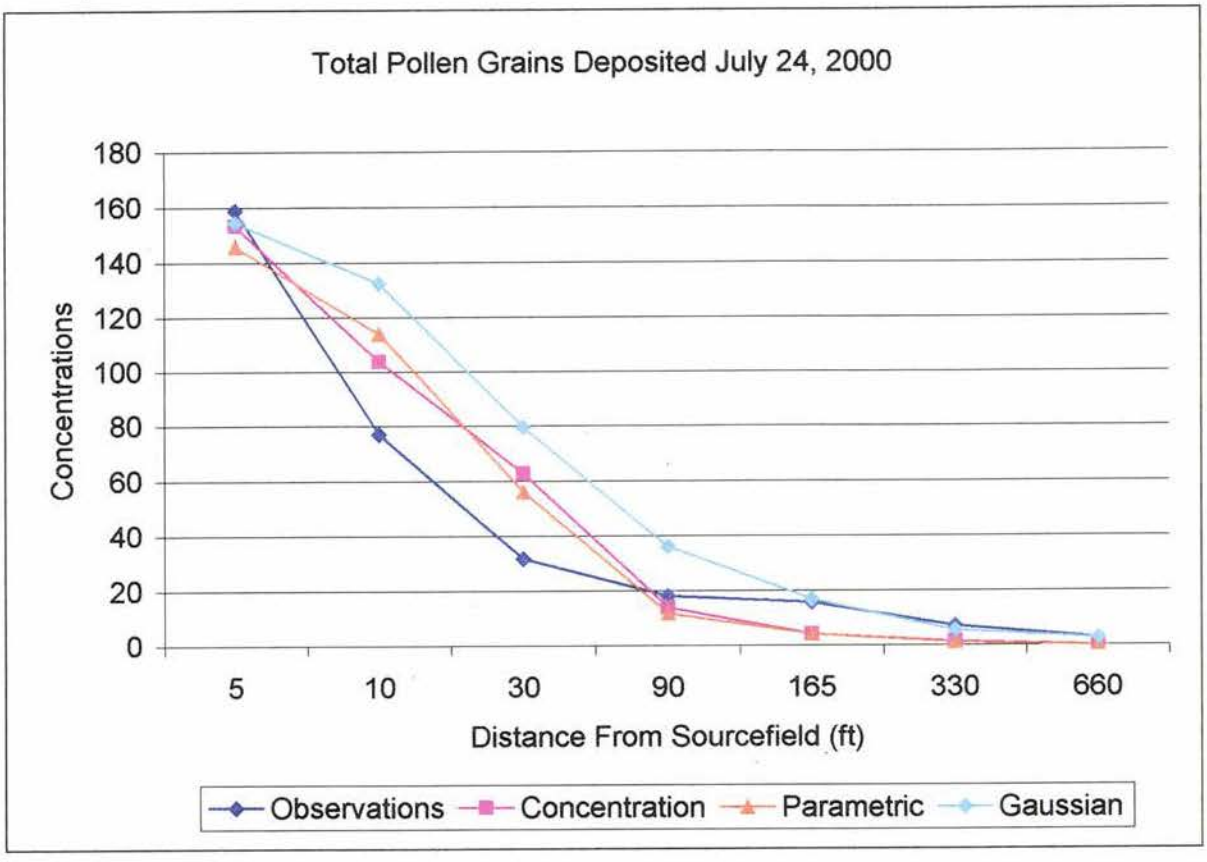

Figure 5.11. The July 24, 2000 deposition profile of all the axes over the distance away from the source field. The deposition is given in grains cm^{-2}.

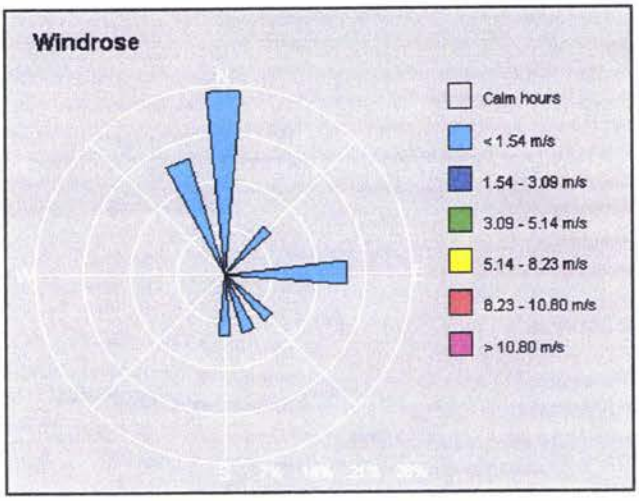

Figure 5.12. The wind rose for July 27, 2000 (Ashton et al. 2000).

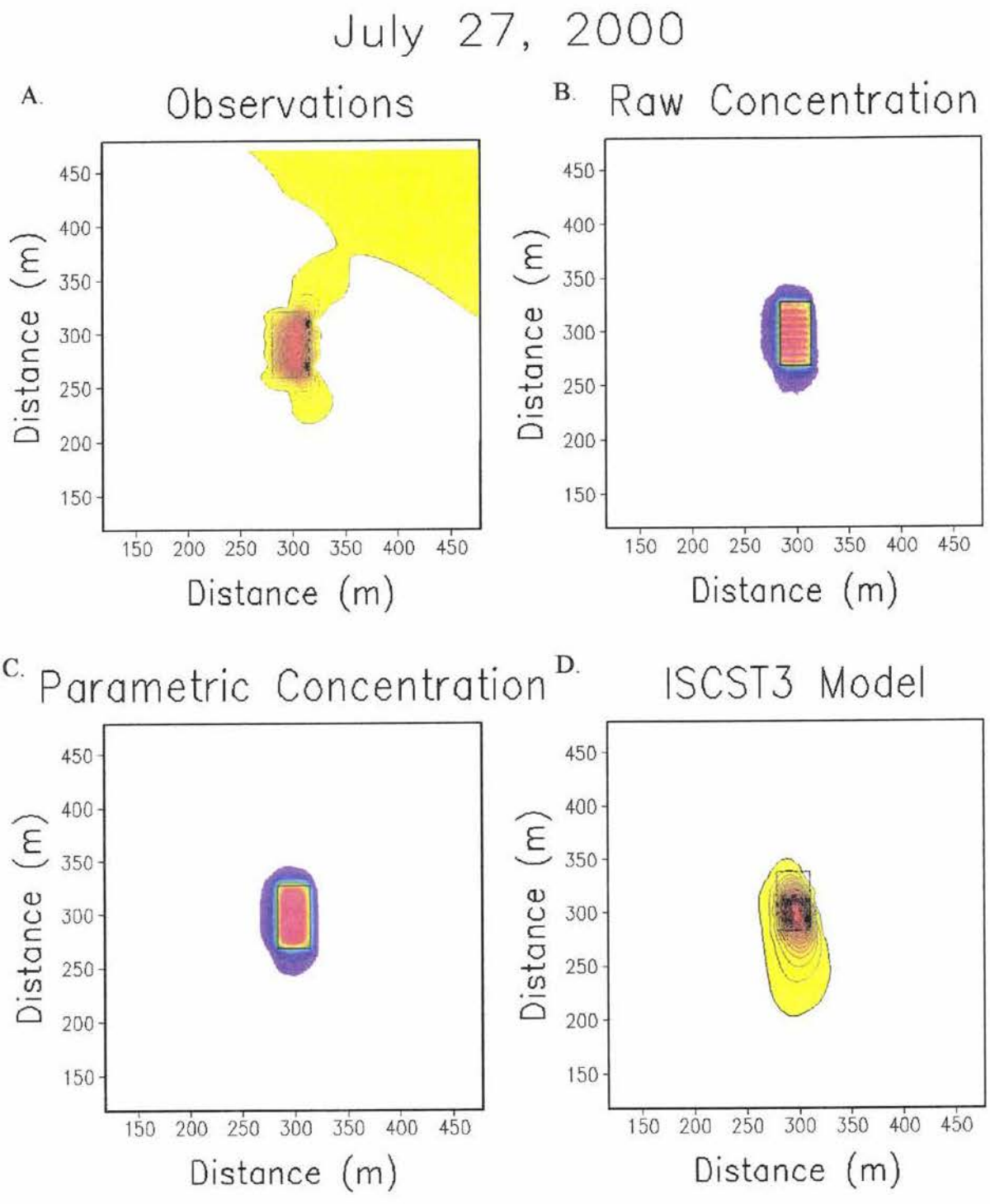

Figure 5.13. (A) Observed pollen counts (Ashton et al. 2000), the Lagrangian pollen dispersion model's predicted (B) raw concentrations and (C) parametric concentrations, and the (D) ISCST3's (Ashton et al. 2000) predicted concentrations for July 27, 2000. The rectangle is the source field.

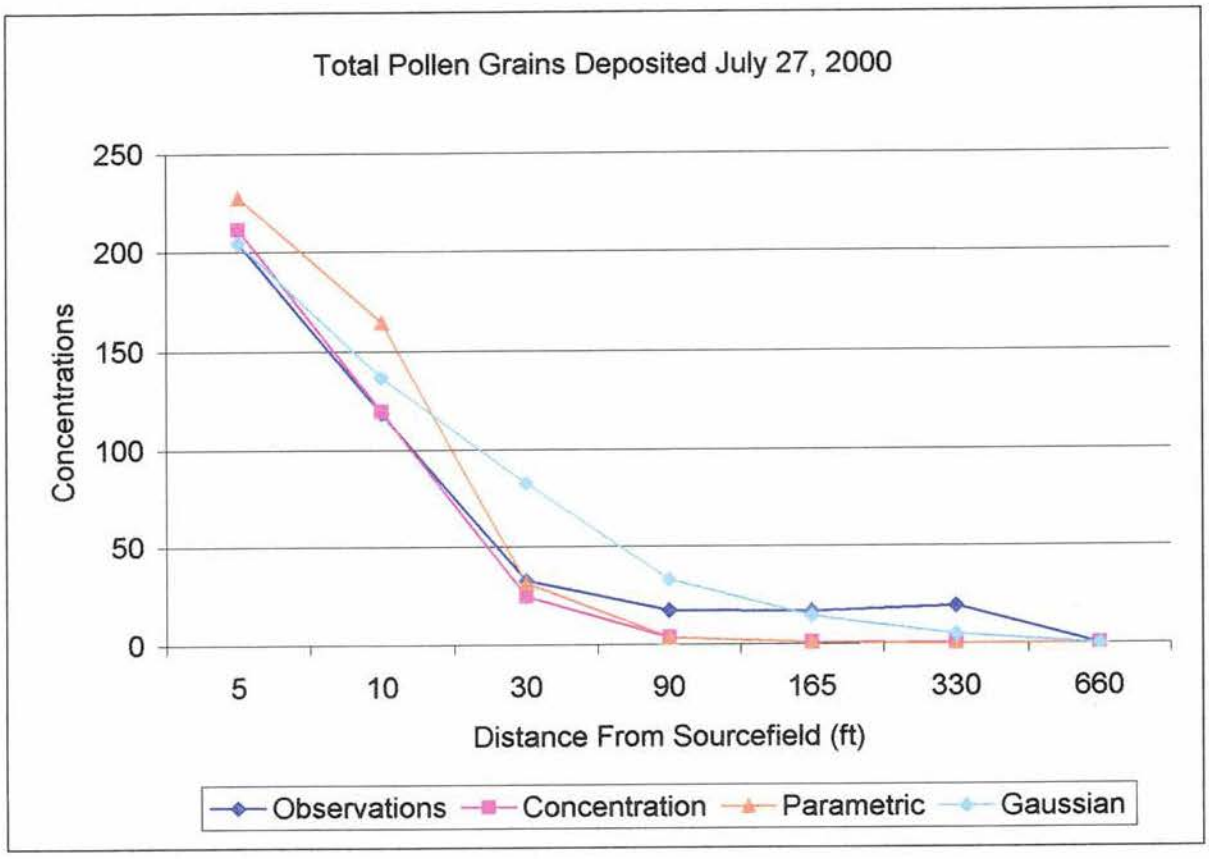

Figure 5.14. The July 27, 2000 deposition profile of all the axes over the distance away from the source field. The deposition is given in grains cm^{-2}.

CHAPTER 6. PARTICLE SIZE DISTRIBUTION

The dispersion of maize pollen is influenced by its large size. Maize pollen is among the largest pollen in the grass family with a diameter of approximately 80 – 100 μm. The average pollen grain has a volume of 700×10^{-9} cm^3 and weighs 247×10^{-9} g (Emberlin et al. 1999). A typical maize pollen grain terminal fall speed is 0.20 m s^{-1} (Emberlin et al. 1999; Raynor et al. 1972).

Pollen grains come in a distribution of sizes; these sizes will have different terminal fall speeds associated with them. Large pollen grains will have larger terminal fall speeds than small pollen grains. This means that large pollen grains should travel shorter than smaller pollen grains.

6.1 Introduction to Pollen Size

The Reynolds number is the ratio of inertial force (storage of momentum) to viscous force, given by:

$$\mathrm{Re} = \frac{F_i}{F_\upsilon}.$$

The inertial force is:

$$F_i = \frac{v^2}{d}$$

where v is the terminal velocity of the pollen grain and d is the diameter of the pollen grain. The viscous force is:

$$F_\nu = \nu \frac{v}{d^2} \text{ where } \nu = \frac{\mu}{\rho_f}$$

where ν is kinematic viscosity, μ is dynamic molecular viscosity of air, and ρ_f is the density of the air. Substituting variables in for the inertial force (F_i) and viscous force (F_ν) the equation is:

$$Re = \frac{\rho_f dv}{\mu}$$

where Re is the Reynolds number, ρ_f is the density of air ($1.2\ kg\ m^{-3}$), μ is dynamic molecular viscosity of air ($1.789 \times 10^{-5}\ kg\ m^{-1}\ s^{-1}$), d is the diameter of the pollen grain (an average of 8×10^{-5} m) and v is the terminal fall speed of the pollen grain (an average of $0.2\ m\ s^{-1}$). Substituting these values into the Reynolds number equation yields approximately 1.0.

It is possible to predict the terminal velocity of pollen grains using Stokes' Law. Stokes' Law is given by:

$$F_g = F_d$$

where F_g is the gravitational force and F_d is the drag (or frictional) force. The gravitational force on the pollen grain is equal to:

$$F_g = \frac{\pi \rho d^3 g}{6}$$

where g is gravitational acceleration ($9.8\ m\ s^{-2}$), and ρ is the density of the pollen grain (set to $1.3 \times 10^3\ kg\ m^{-3}$). The frictional force the pollen grain exerts on the air is:

$$F_d = 3\pi dv\mu$$

where v is the terminal fall speed and μ is the dynamic molecular viscosity of air. Set the gravitational force equal to the frictional force and solve for v to get the equation for the terminal velocity:

$$v = \frac{\rho g d^2}{18\mu}.$$

Figure 6.1 shows the variation in terminal velocity with increasing radii of pollen grains. Using Westgate and Fonseca's data and calculating the terminal fall speed with the above equation the average terminal fall speed is $0.24\ m\ s^{-1}$ with the standard deviation of $0.035\ m\ s^{-1}$.

Westgate and Fonseca's data were found by collecting pollen grains in Isoton II solution. The pollen grains were counted using a Coulter Multisizer II, which was set to count particles between 60 and 100 μm (the size of pollen grains) in diameter. The Coulter Multisizer II counts particles going through a probe using electroconductivity. The multisizer then gives the user the number of particles (in this case pollen grains) and the average size for the particles (Agustin Fonseca, personal communication). Using the average pollen grain size and the standard deviation it is possible to change the uniform terminal fall speed for all pollen particles to a distribution related to that of the actual pollen sizes using Stokes' Law, relevant to Reynolds numbers close to 1.0.

There were three sensitivity model runs with three different pollen grain sizes. The first one uses a distribution of pollen sizes from data collected by Mark Westgate and Agustin Fonseca. The second one sets all the terminal fall speeds of the pollen grains to one standard deviation above the mean, 0.27 m s^{-1} (for large pollen grain sizes). The third one sets all the terminal fall speeds of the pollen grains to one standard deviation below the mean, 0.20 m s^{-1} (for small pollen grain sizes). Since the four verification model runs used a terminal fall speed of 0.20 m s^{-1}, the small pollen grain model run is the same as the July 21, 2000 verification run.

The sensitivity tests on the pollen grain size used data from July 21, 2000 because the wind direction and speed stayed steady throughout the day. The average wind direction for July 21, 2000 from 8:00 local time to 17:00 local time was 337° and the average wind speed was 2.6 m s^{-1}. The wind rose for July 21, 2000 is shown in Figure 5.3.

The pollen grain size sensitivities use ten individual model runs for each day, set up like the verification model runs. Each model run uses the average sensible heat flux, wind speed, and direction for that hour. These ten runs are one hour long for each of the ten hours that pollen released. The pollen grains are released for the first fifty minutes of each model run, allowing ten minutes for the pollen grains to land on the ground or go out of the model domain area. The ten runs are multiplied by the percentage of the diurnal pollen shed shown in Figure 5.2. The graph shows the

estimated pollen shed which occurs for ten hours (8:00 local time to 17:00 local time) and the peak emission occurs at 11:00 local time (Westgate, unpublished).

6.2 Results

Figures 6.2, 6.3, and 6.4 show the pollen concentrations for the pollen size distribution, large pollen size, and small pollen size respectively. These figures show that the pollen grains with a terminal fall speed set to 0.20 m s^{-1} (the small pollen grains) traveled slightly farther than the pollen grains with varying terminal fall speed. The pollen grains with varying terminal fall speed traveled slightly farther than the pollen grains with a terminal fall speed set to 0.27 m s^{-1} (the large pollen grains). This is expected, since a smaller terminal fall speed will allow pollen grains to stay in the air longer than larger terminal fall speeds, hence allowing the pollen grains to travel farther from the source field.

The deposition profiles over all axes of the pollen size distribution, large pollen size, and small pollen size are shown in Figures 6.5, 6.6, and 6.7 respectively. The model runs all deposit too many pollen grains close to the source field and not enough farther away. The pollen size distribution model run matched up the best with the observations. This shows that when running the models a pollen size distribution should be used to give a better representation of the pollen deposition field. All of the model runs had all of the pollen being deposited before 330 ft from the source field and the observations showed pollen being deposited as far as 660 ft.

The correlations of the pollen size model runs versus the observations are shown in Table 6.1. It is interesting to note that the three pollen size distribution and large pollen size model runs have higher r^2 values than the small pollen size model run when compared with the July 21, 2000 observations. This is interesting because the small pollen size model run used the terminal fall speed thought to be the average terminal fall speed of maize pollen grain, yet the model runs that used other

terminal fall speeds could explain more of the variance than the model run with a small terminal fall speed.

Table 6.2 shows the percentage deposition of pollen grains in the source field. This table shows all of the raw concentrations from the pollen size sensitivity testing model runs match up closely with the observations, with the pollen size distribution and large pollen size model runs the closest to the observations.

Overall, the pollen size distribution matched up the best with the observations than the other two pollen size model runs. In future work, a pollen size distribution should be used in the pollen dispersion model to better represent what occurs in the field.

Table 6.1. R^2 values for the Lagrangian pollen dispersion model with a pollen size distribution, a large pollen size, and a small pollen size. All values are significant at the 99% level.

	Lagrangian	
	raw	parametric
Distribution	0.802	0.782
Large	0.795	0.789
Small	0.774	0.774

Table 6.2. The percentage of pollen grains deposited in the source field.

	% of pollen grains in the source field	
	raw	parametric
Distribution	90%	87%
Large	90%	88%
Small	89%	87%

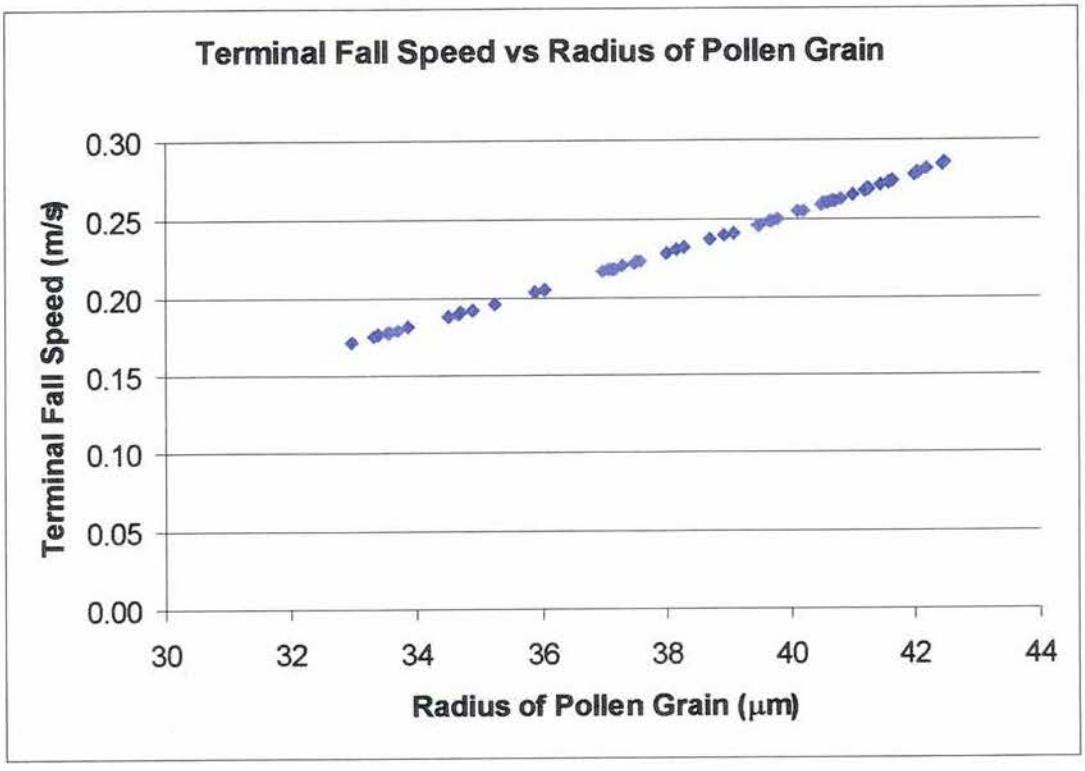

Figure 6.1. Shows the terminal fall speed versus the radius size of maize pollen grains.

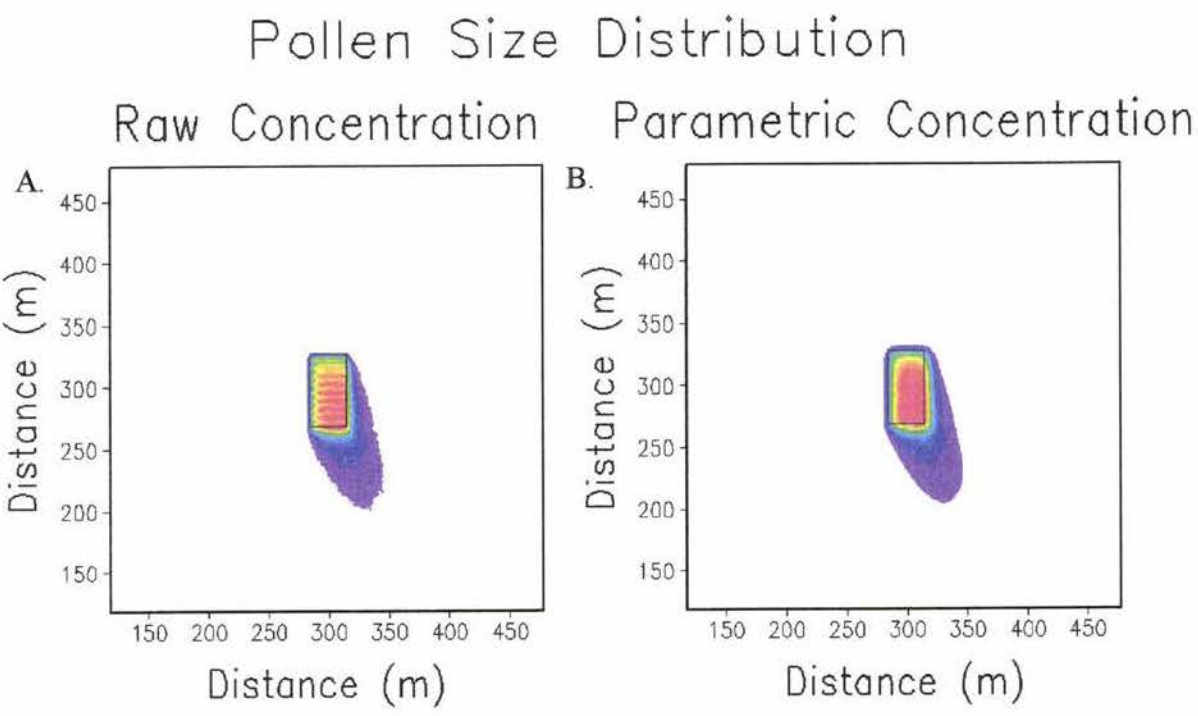

Figure 6.2. The Lagrangian pollen dispersion model's predicted (A) raw concentrations and (B) parametric concentrations using a pollen size distribution with the average (0.24 m s^{-1}) and standard deviation (0.035 m s^{-1}) of pollen sizes.

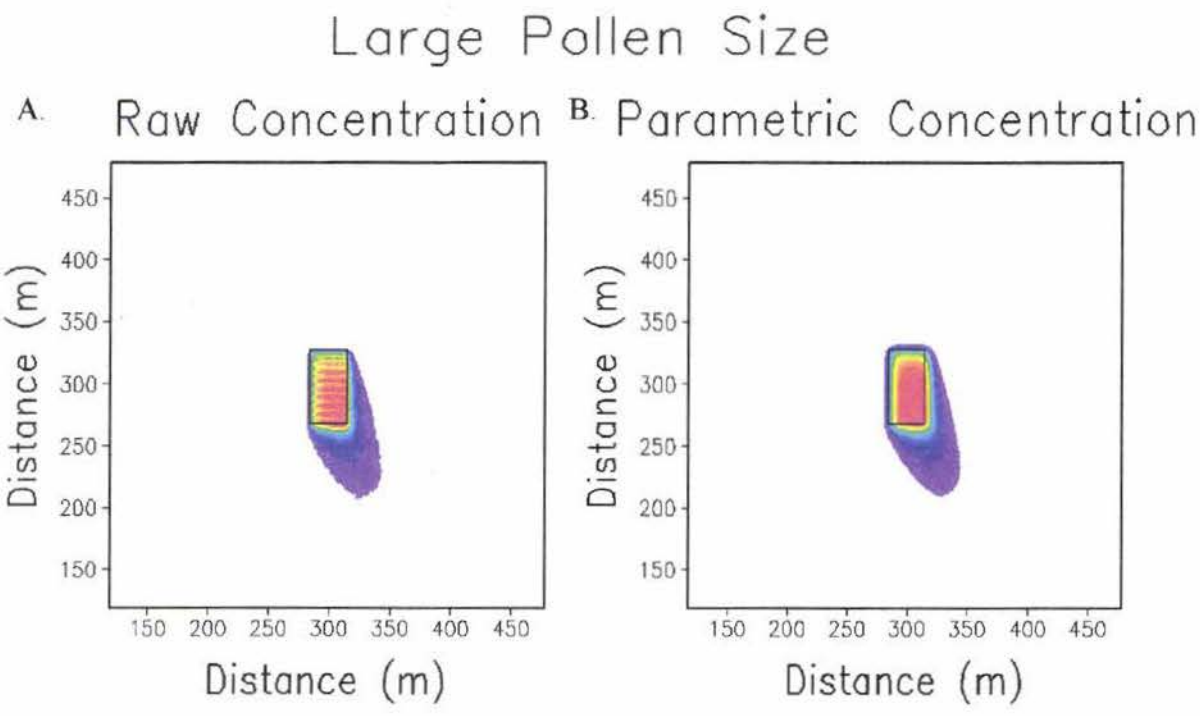

Figure 6.3. The Lagrangian pollen dispersion model's predicted (A) raw concentrations and (B) parametric concentrations with a large pollen size (large terminal fall speed) of one standard deviation above the average pollen size (0.27 m s^{-1}).

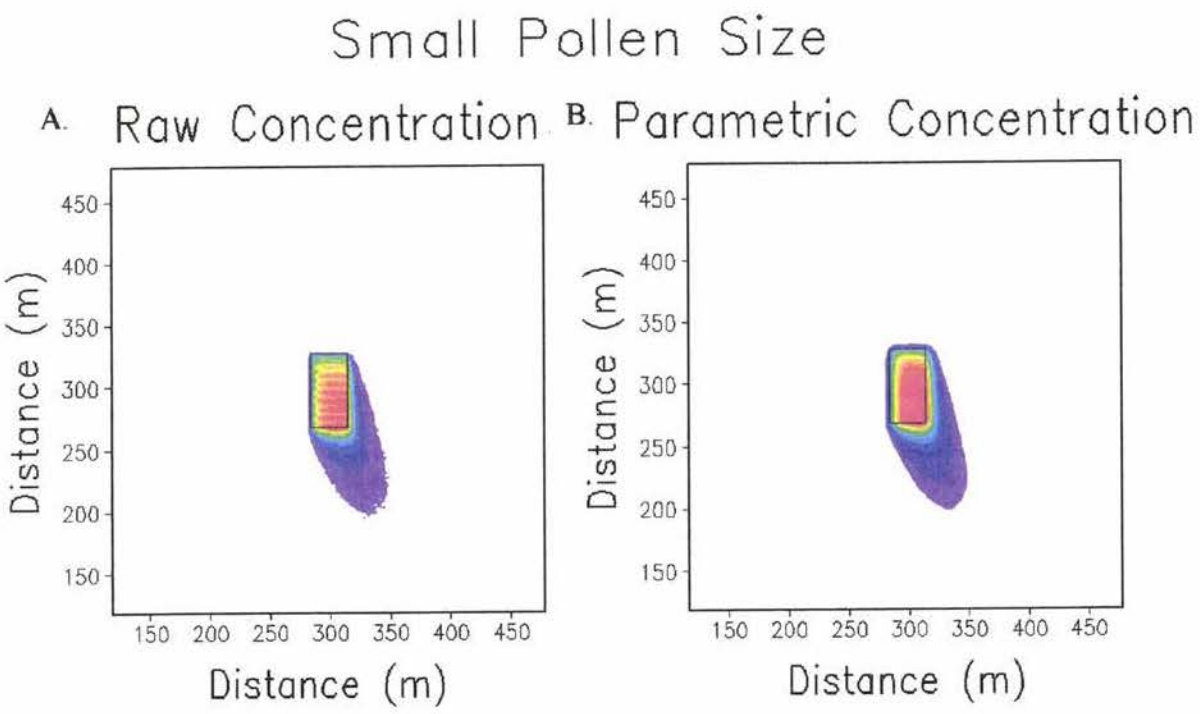

Figure 6.4. The Lagrangian pollen dispersion model's predicted (A) raw concentrations and (B) parametric concentrations with a small pollen size (small terminal fall speed) of one standard deviation below the average pollen size (0.20 m s^{-1}).

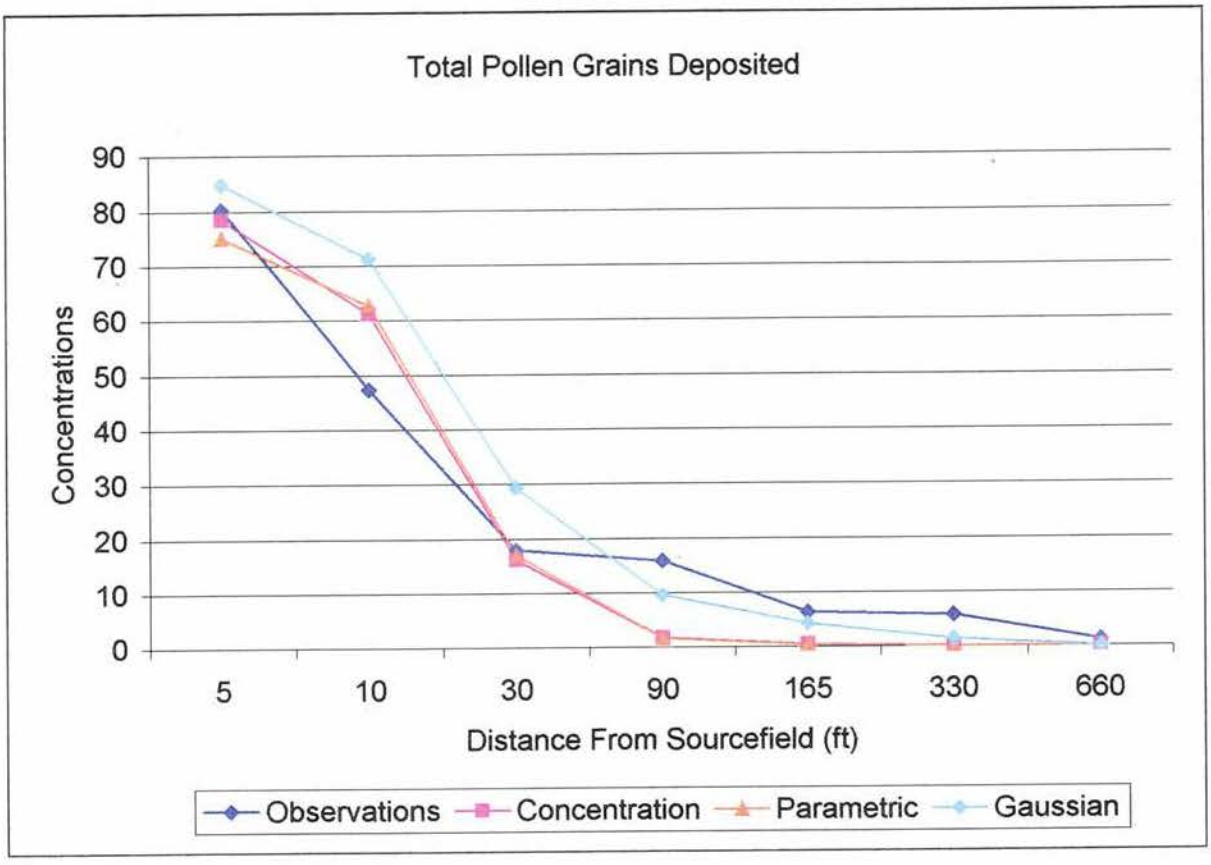

Figure 6.5. The deposition profile of all the axes over the distance away from the source field for a pollen size distribution using the average and standard deviation of pollen sizes. The deposition is given in grains cm^{-2}.

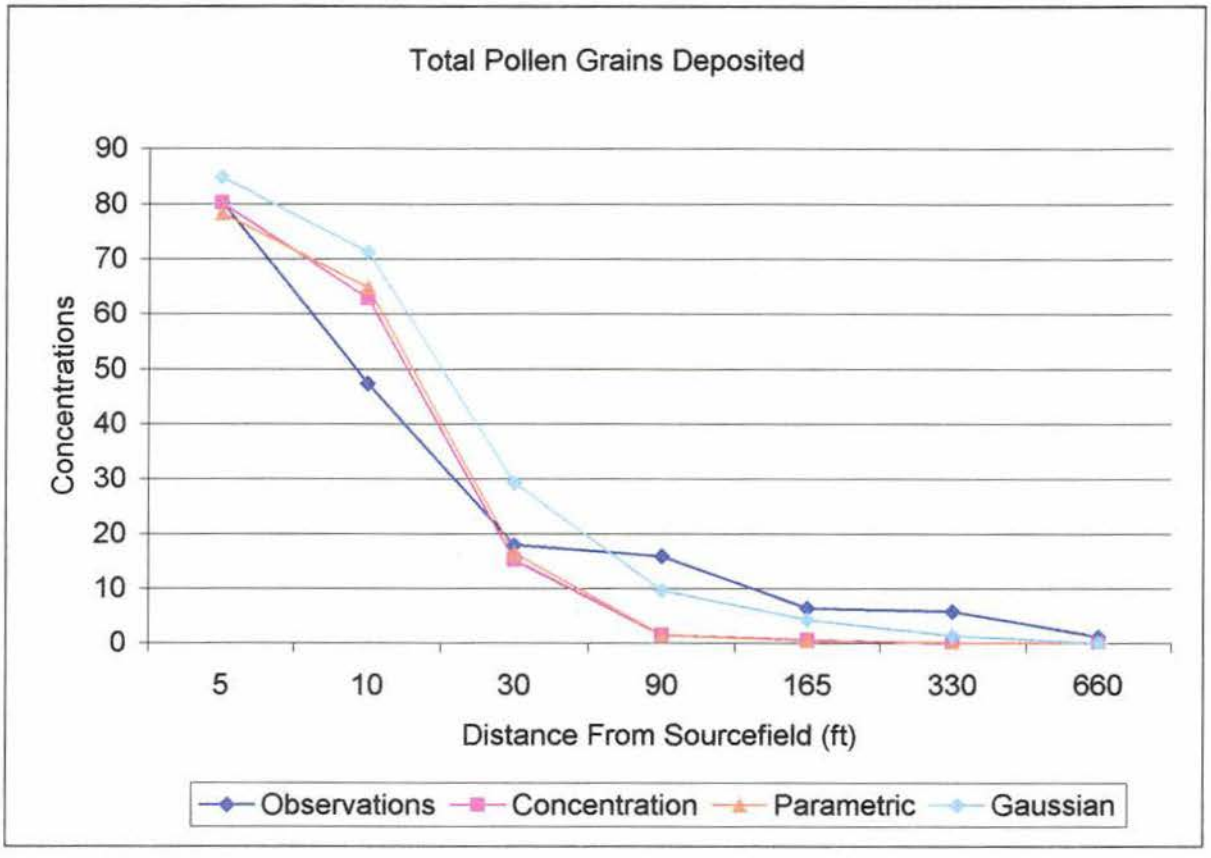

Figure 6.6. The deposition profile of all the axes over the distance away from the source field for a large pollen size with a terminal fall speed of one standard deviation above the average of pollen sizes. The deposition is given in grains cm^{-2}.

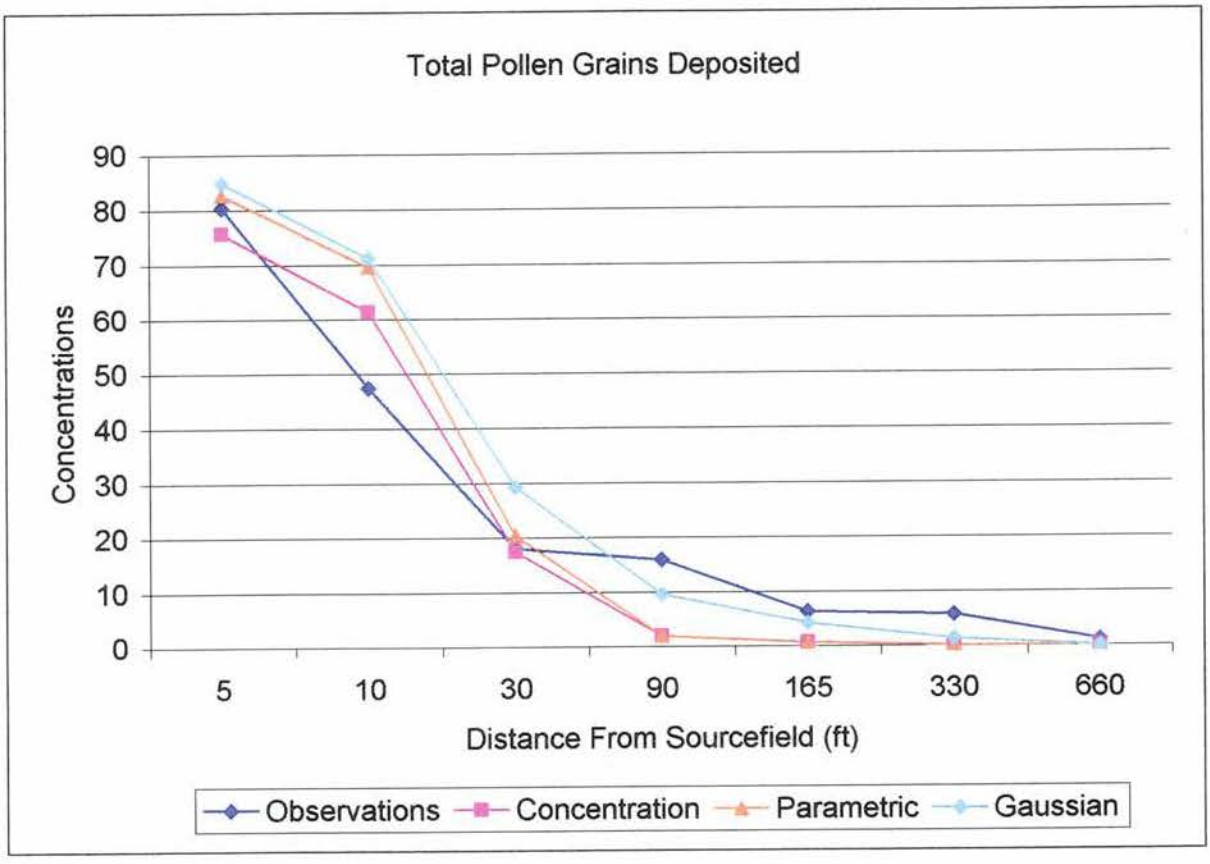

Figure 6.7. The deposition profile of all the axes over the distance away from the source field for a small pollen size with a terminal fall speed of one standard deviation below the average of pollen sizes. The deposition is given in grains cm^{-2}.

CHAPTER 7. EFFECTS OF ENVIRONMENTAL CONDITIONS

Wind speed and atmospheric stability were varied to determine how pollen dispersion reacts to different weather conditions. With stronger wind speeds it is expected that pollen grains will be deposited farther downwind than with lighter wind speeds. With stronger atmospheric instability it is expected that pollen grains will be deposited farther downwind than with weak atmospheric instability or neutral atmospheric stability.

7.1 Introduction to the Effects of Environmental Conditions

The wind speeds in the sensitivity testing are 0.5 m s^{-1}, 1.0 m s^{-1}, 2.0 m s^{-1}, 4.0 m s^{-1}, and 8.0 m s^{-1}. To change the atmospheric stability, the sensible heat flux input to the model is changed from neutral conditions (0 W m^{-2}), to 25 W m^{-2}, 50 W m^{-2}, and 100 W m^{-2} for weakly, moderately, and strongly unstable conditions, respectively. The larger the sensible heat flux the more heating is created at the surface and the atmospheric conditions become unstable. The sensitivity tests are done using a constant wind direction to ensure a controlled experiment. Therefore, the sensitivity tests use field observations from July 21, 2000, because on this day there was the least variability in wind direction.

A matrix was used to study how changes in both wind speed and atmospheric stability affect pollen dispersion. By using the matrix it can be determined how wind speed and atmospheric stability work together when moving pollen grains through the air. The model was run at one wind speed to test the impact of atmospheric stability with neutral, weakly unstable, moderately unstable, and strongly unstable conditions. Then, the wind speed was changed and again the model was run for varying atmospheric stability for neutral, to weakly unstable, moderately unstable, and strongly unstable.

7.2 Results

Figures 7.1 to 7.10 show the pollen concentrations for all of the varying wind speeds and atmospheric conditions runs. These figures show that the stronger the wind speed the farther from the source field the pollen grains are deposited. At low wind speeds (0.5 m s^{-1} and 1.0 m s^{-1}) the stronger the instability the farther from the source field the pollen grains are deposited. When the wind speeds are stronger (2.0 m s^{-1}, 4.0 m s^{-1}, and 8.0 m s^{-1}) there is no noticeable difference in the distance pollen grains are deposited from the source with instability.

The deposition profiles over all axes are shown in Figures 7.11 to 7.15. For all runs there was no deposition past 90 ft. This might occur because none of the axes corresponded to the direction of the wind. If one of the axes was the same as the wind direction (330°) there might have been pollen at all distances. At the low wind speeds (0.5 and 1.0 m s^{-1}) the deposition profiles are close to the observations at 5 feet and 10 feet and underestimate at 30 feet and 60 feet away from the source field. At 2.0 m s^{-1} the model was close at 5 feet and 30 feet, overestimated at 10 feet, and underestimated at 60 feet away from the source field. For the strong wind cases (4.0 and 8.0 m s^{-1}) again the model was close at 5 feet and 30 feet, overestimated at 10 feet, and underestimated at 60 feet away from the source field.

When the stability is considered, only for the lightest wind speed (0.5 m s^{-1}) is there a change in the deposition profile. These could be a result from the axes that the observations were taken did not correspond to the wind direction, which is where the most amount of variability would occur in the model runs. Another result could be in the scaling factors used.

Tables 7.1 and 7.2 show the percentage of pollen grains deposited in the source field over all pollen grains deposited for the raw concentrations and parametric concentrations respectively. With stronger wind speeds fewer pollen grains are deposited in the source field and with stronger the instability fewer pollen grains are deposited in the source field. The only model run that matched up with the July 21, 2000 observations (92%) is the 1 m s^{-1} raw concentration model runs with neutral

stability. The lower wind speed model runs had more pollen grains deposited in the source field than the higher wind speed model runs. This is expected because the stronger wind speeds will push the pollen grains farther downwind faster than the lower wind speeds. With the lower wind speeds (0.5, 1.0, and 2.0 m s^{-1}) the neutral stability model runs had more pollen grains deposited in the source field than the instability cases. This is expected since the instability cases should carry the pollen grains farther from their source.

Table 7.1. The percentage of pollen grains deposited in the source field for all the raw concentrations atmospheric stability and wind speed model runs.

Wind Speed	Stability			
	Neutral	Weak Instability	Moderate Instability	Strong Instability
.5 ms^{-1}	95%	94%	93%	93%
1 ms^{-1}	92%	91%	91%	91%
2 ms^{-1}	90%	90%	89%	89%
4 ms^{-1}	87%	87%	87%	87%
8 ms^{-1}	87%	87%	87%	87%

Table 7.2. The percentage of pollen grains deposited in the source field for all the parametric concentrations atmospheric stability and wind speed model runs.

Wind Speed	Stability			
	Neutral	Weak Instability	Moderate Instability	Strong Instability
.5 ms^{-1}	90%	89%	89%	89%
1 ms^{-1}	89%	88%	88%	88%
2 ms^{-1}	87%	87%	87%	87%
4 ms^{-1}	86%	86%	86%	86%
8 ms^{-1}	86%	86%	86%	86%

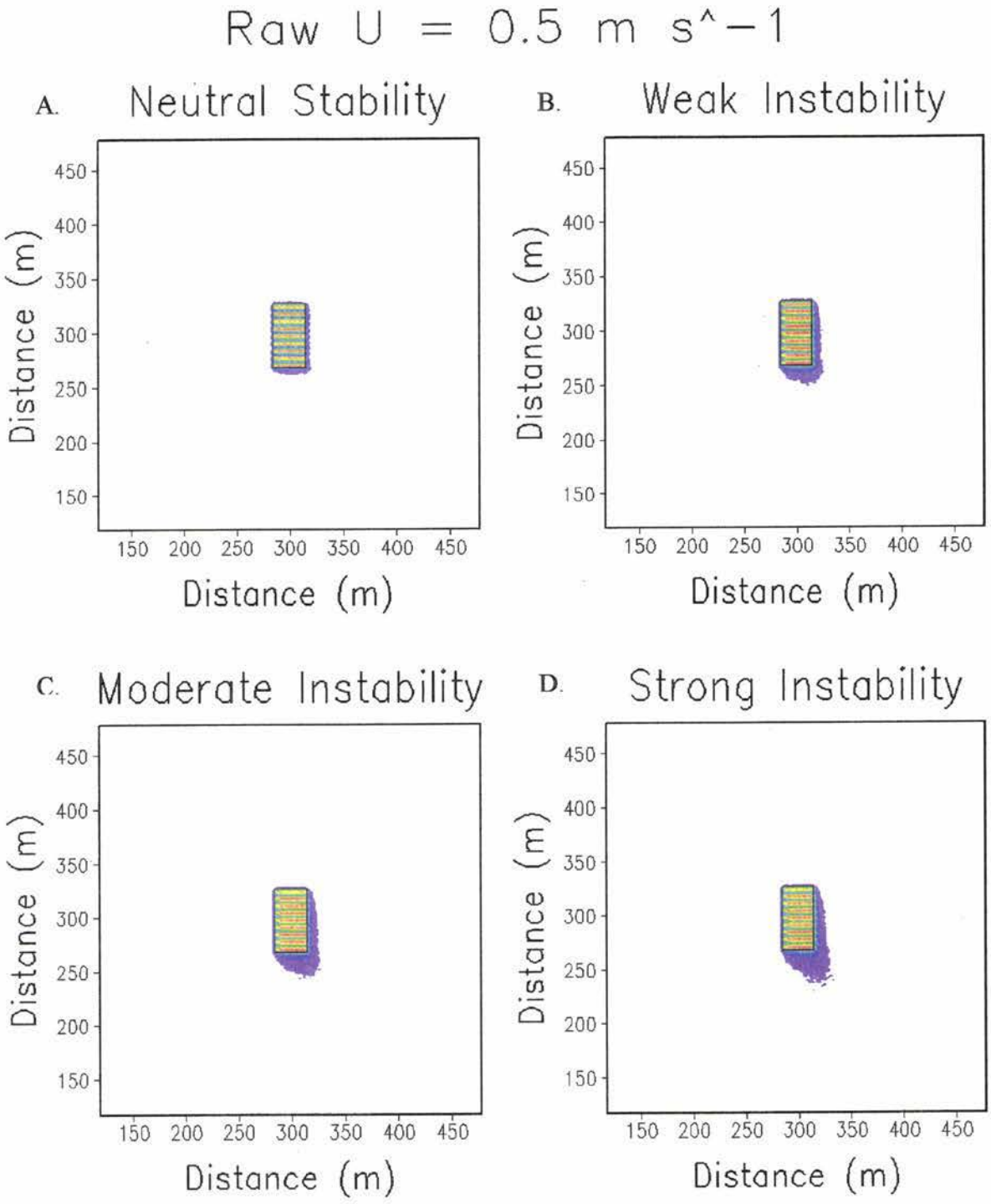

Figure 7.1. The Lagrangian pollen dispersion model's predicted raw concentrations with (A) neutral stability, (B) weak instability, (C) moderate instability, and (D) strong instability and a wind speed of 0.5 m s^{-1}.

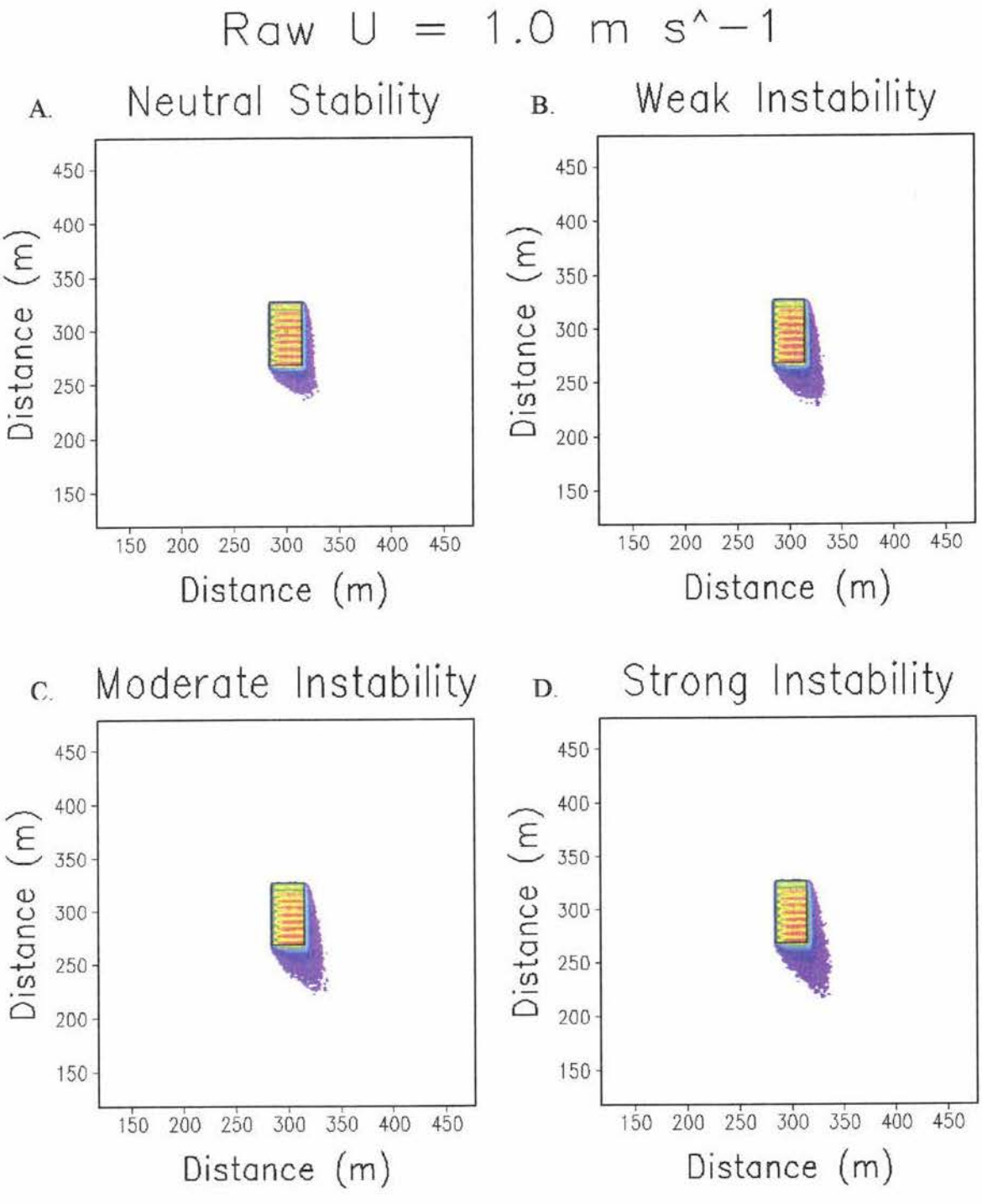

Figure 7.2. The Lagrangian pollen dispersion model's predicted raw concentrations with (A) neutral stability, (B) weak instability, (C) moderate instability, and (D) strong instability and a wind speed of 1.0 m s^{-1}.

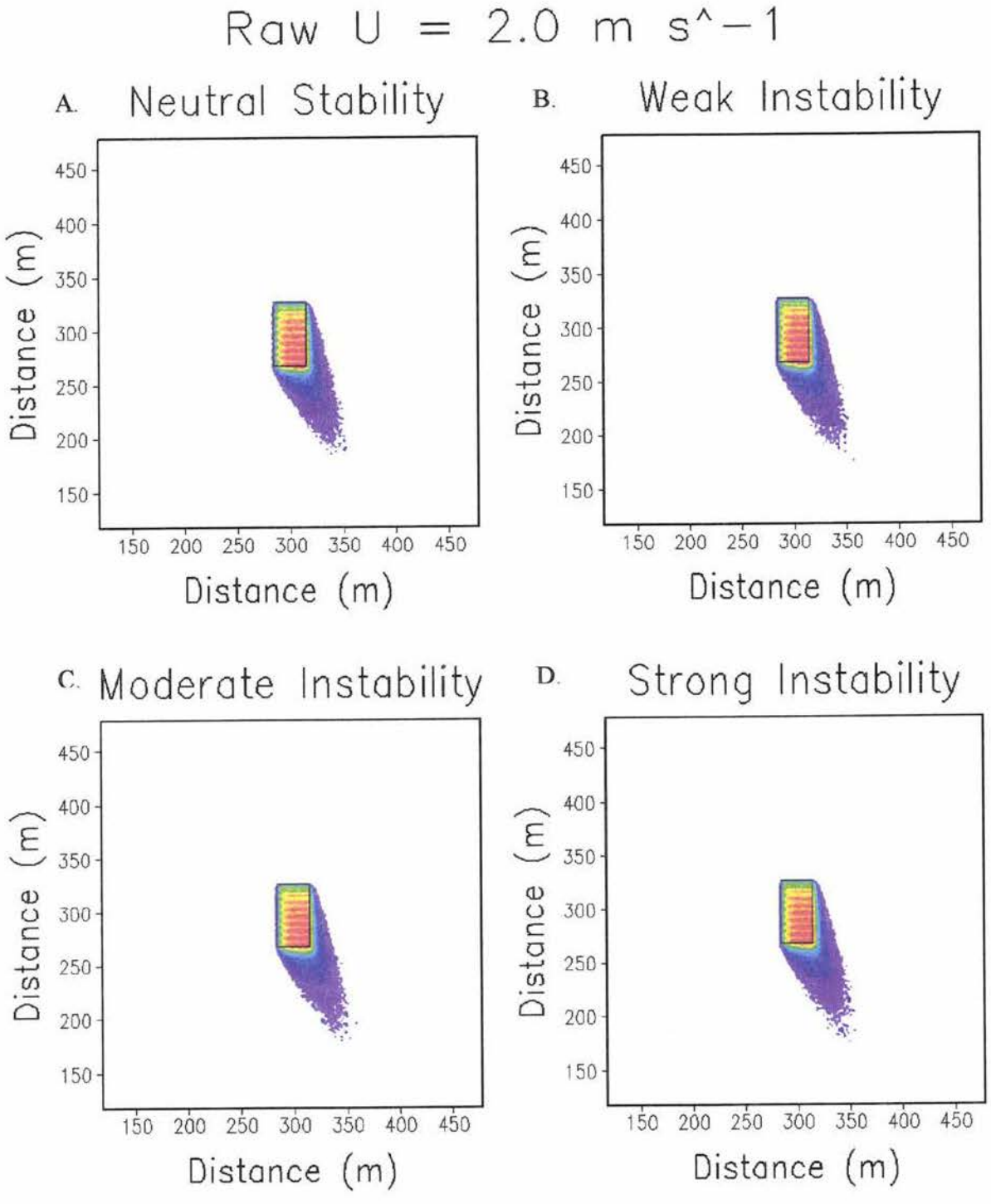

Figure 7.3. The Lagrangian pollen dispersion model's predicted raw concentrations with (A) neutral stability, (B) weak instability, (C) moderate instability, and (D) strong instability and a wind speed of 2.0 m s^{-1}.

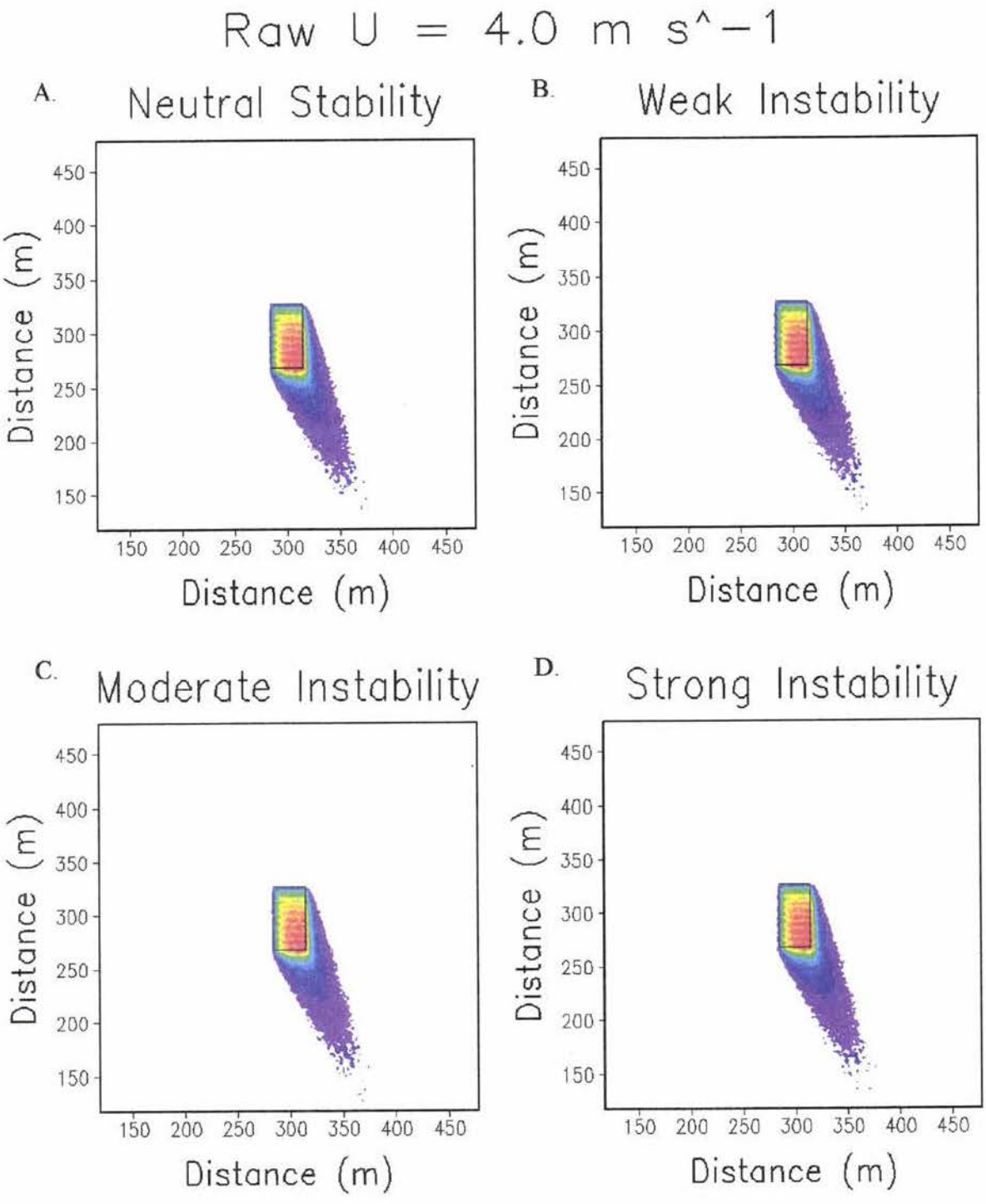

Figure 7.4. The Lagrangian pollen dispersion model's predicted raw concentrations with (A) neutral stability, (B) weak instability, (C) moderate instability, and (D) strong instability and a wind speed of 4.0 m s^{-1}.

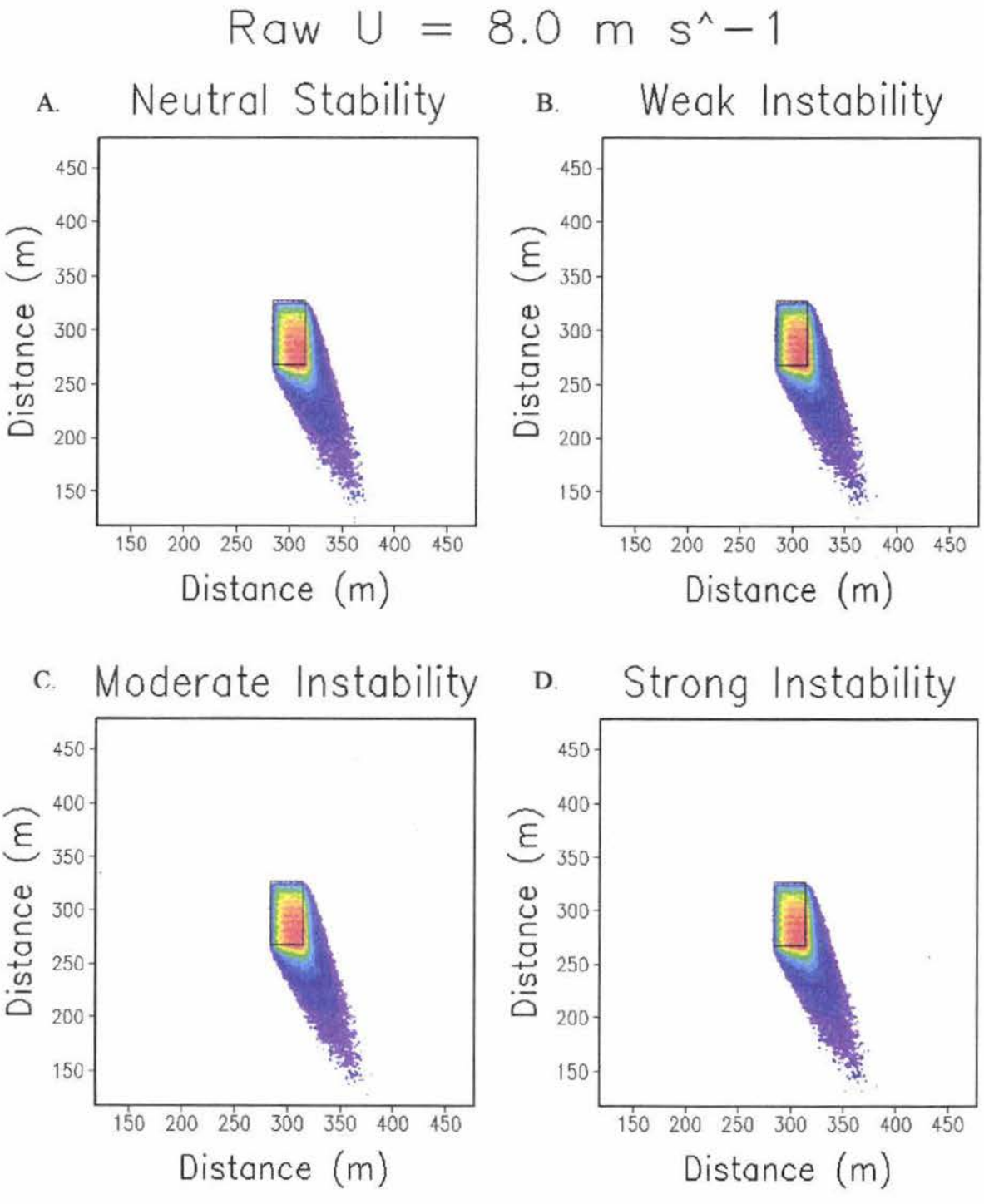

Figure 7.5. The Lagrangian pollen dispersion model's predicted raw concentrations with (A) neutral stability, (B) weak instability, (C) moderate instability, and (D) strong instability and a wind speed of 8.0 m s^{-1}.

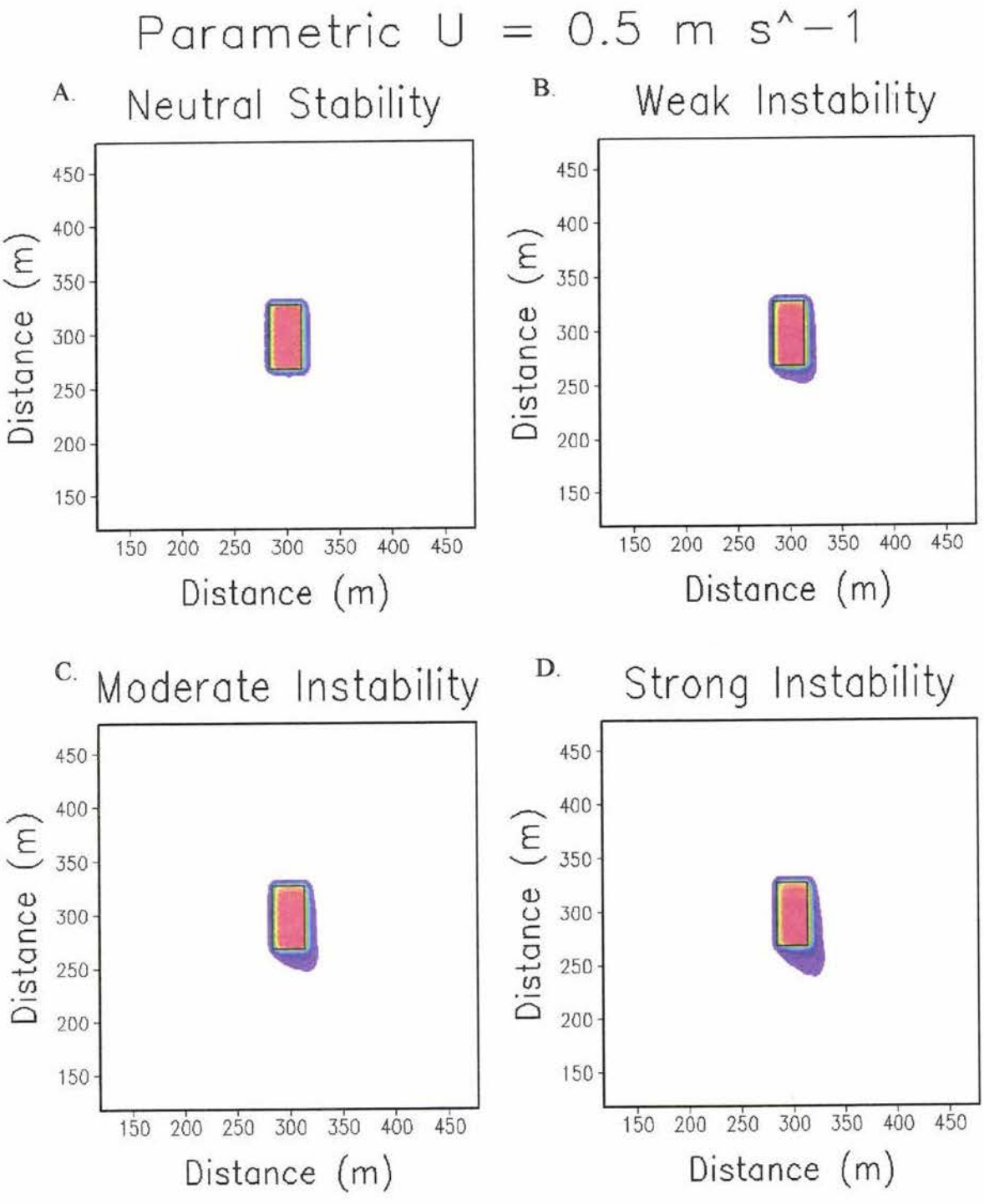

Figure 7.6. The Lagrangian pollen dispersion model's predicted parametric concentrations with (A) neutral stability, (B) weak instability, (C) moderate instability, and (D) strong instability and a wind speed of 0.5 m s^{-1}.

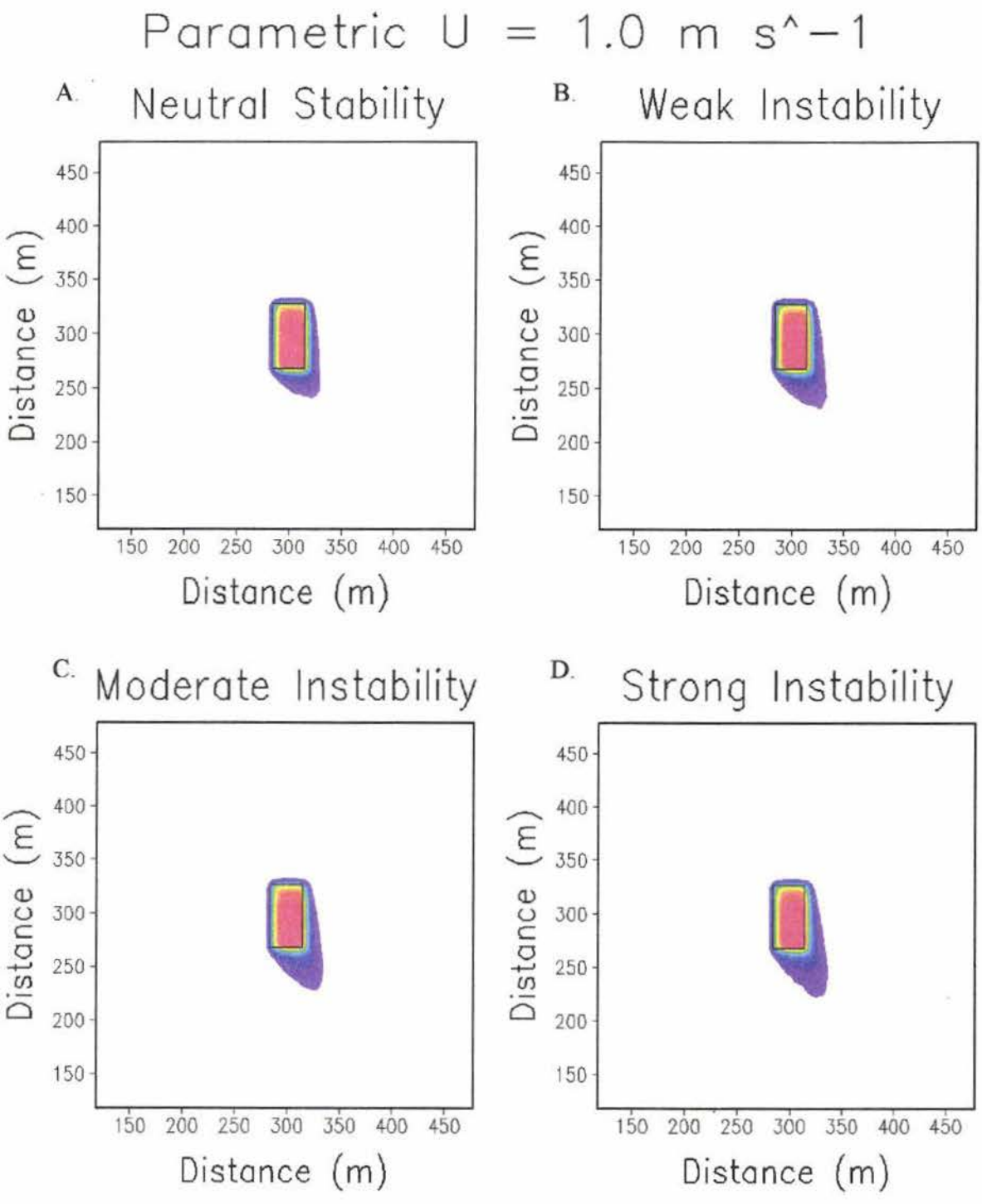

Figure 7.7. The Lagrangian pollen dispersion model's predicted parametric concentrations with (A) neutral stability, (B) weak instability, (C) moderate instability, and (D) strong instability and a wind speed of 1.0 m s^{-1}.

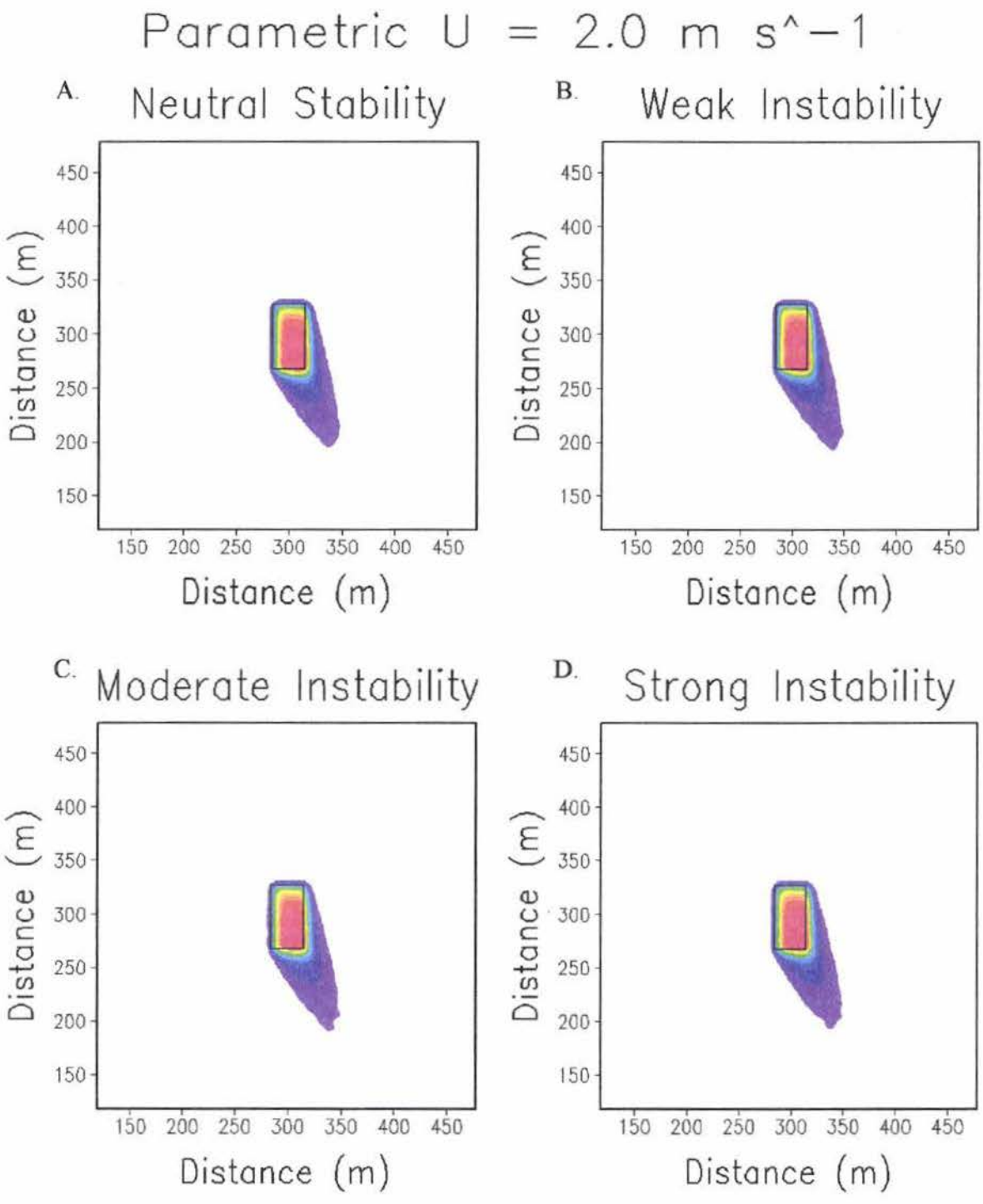

Figure 7.8. The Lagrangian pollen dispersion model's predicted parametric concentrations with (A) neutral stability, (B) weak instability, (C) moderate instability, and (D) strong instability and a wind speed of 2.0 m s^{-1}.

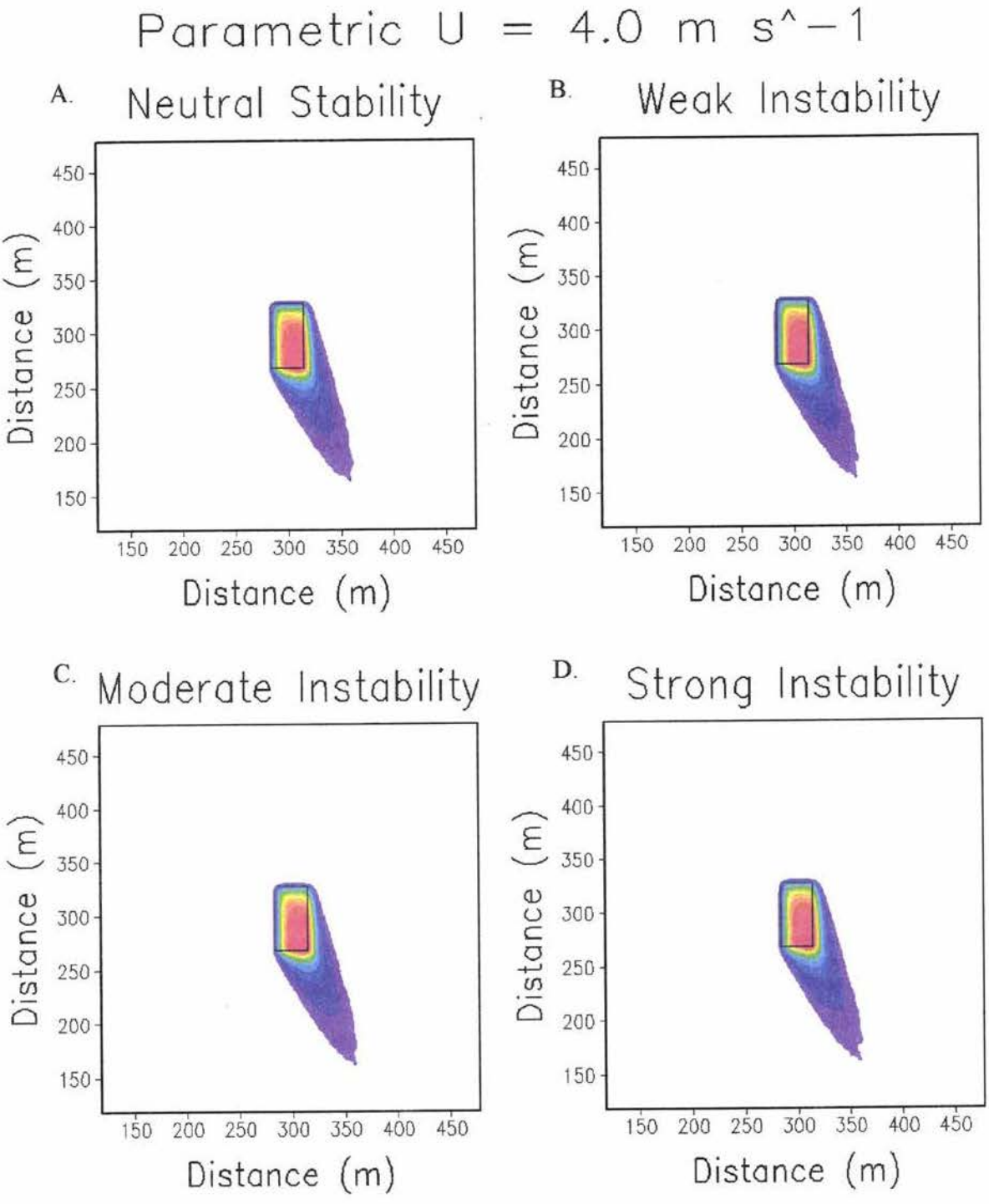

Figure 7.9. The Lagrangian pollen dispersion model's predicted parametric concentrations with (A) neutral stability, (B) weak instability, (C) moderate instability, and (D) strong instability and a wind speed of 4.0 m s^{-1}.

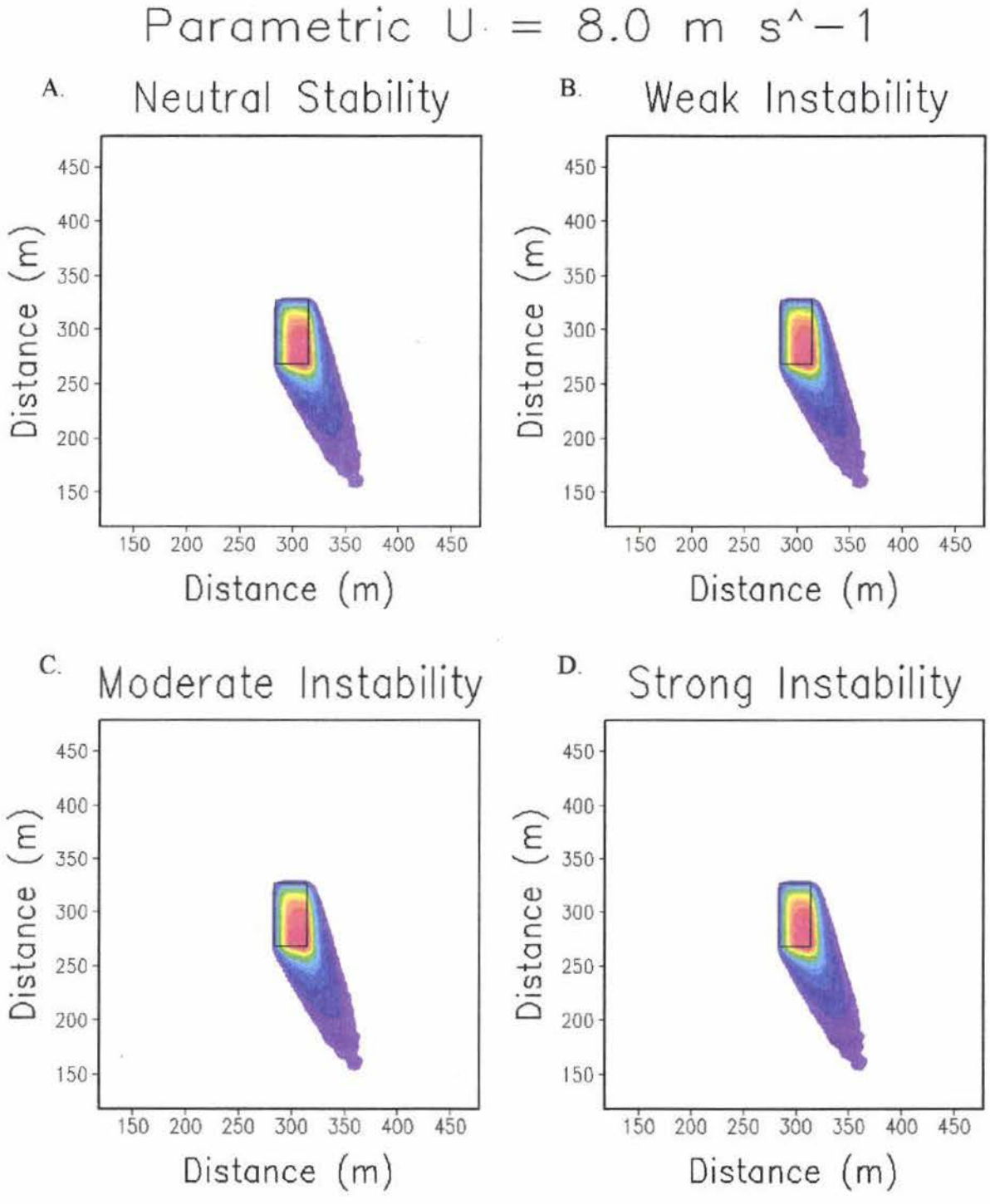

Figure 7.10. The Lagrangian pollen dispersion model's predicted parametric concentrations with (A) neutral stability, (B) weak instability, (C) moderate instability, and (D) strong instability and a wind speed of 8.0 m s^{-1}.

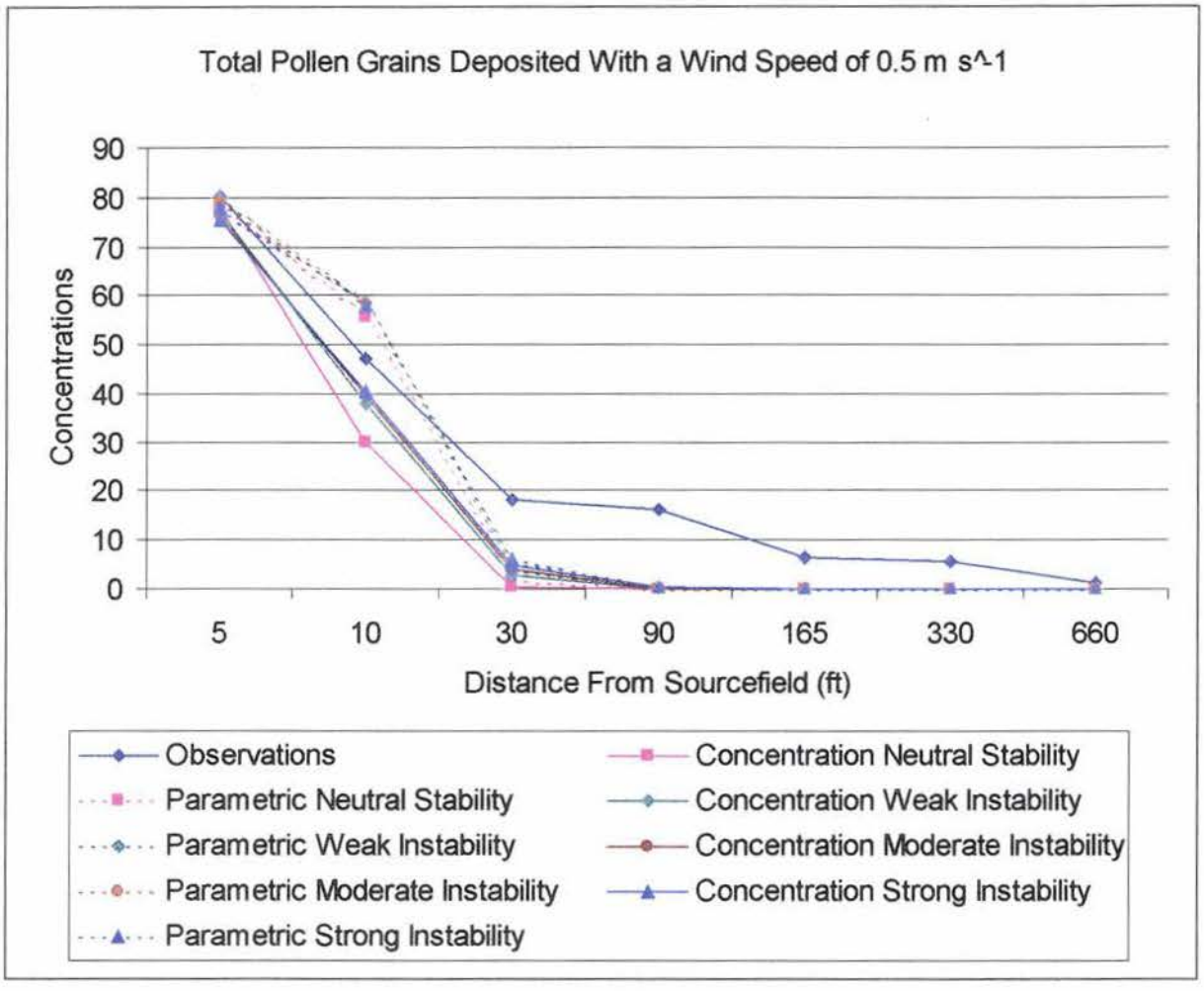

Figure 7.11. The deposition profile of all the axes over the distance away from the source field with a wind speed of 0.5 m s^{-1}. The deposition is given in cm^{-2}.

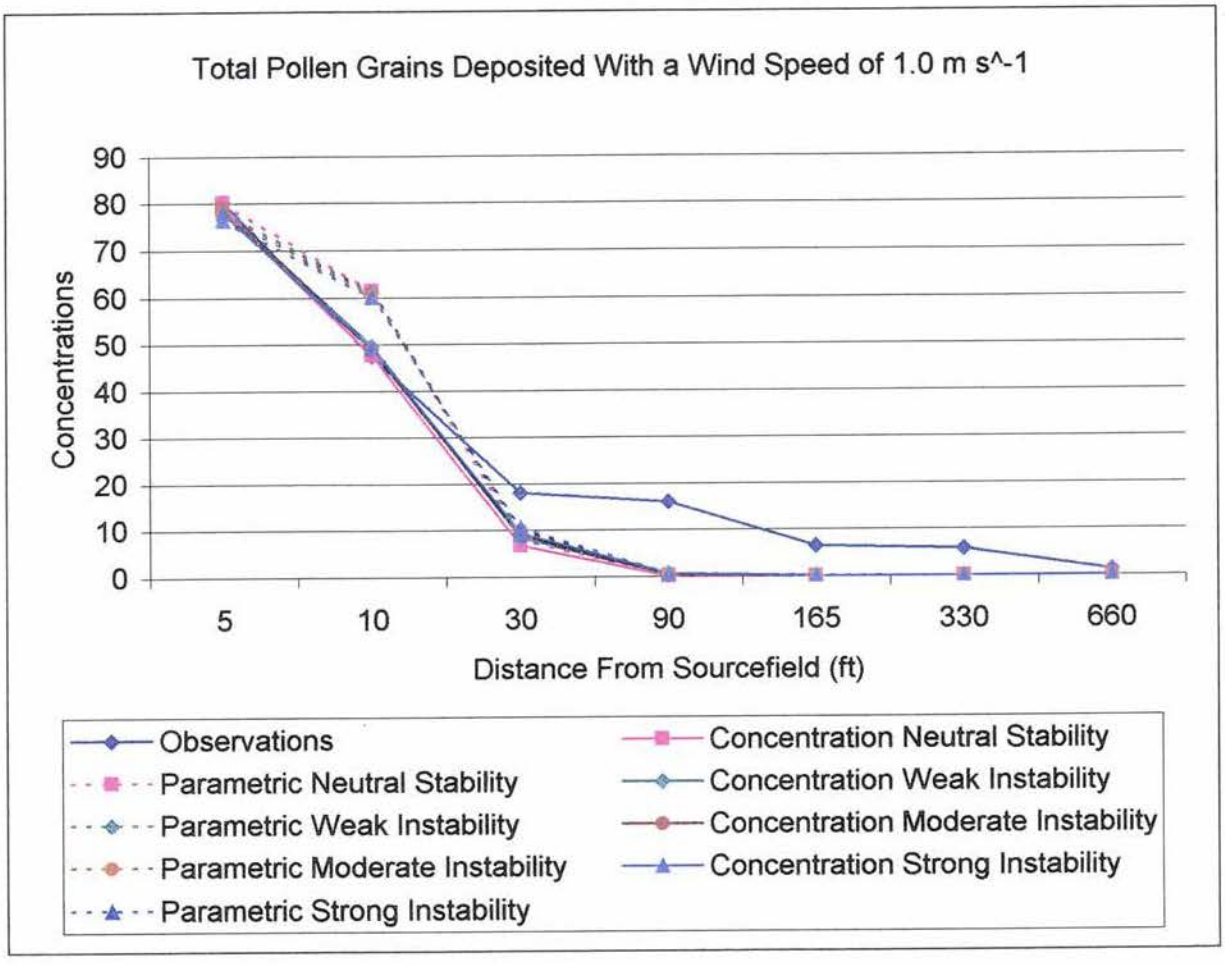

Figure 7.12. The deposition profile of all the axes over the distance away from the source field with a wind speed of 1.0 m s^{-1}. The deposition is given in cm^{-2}.

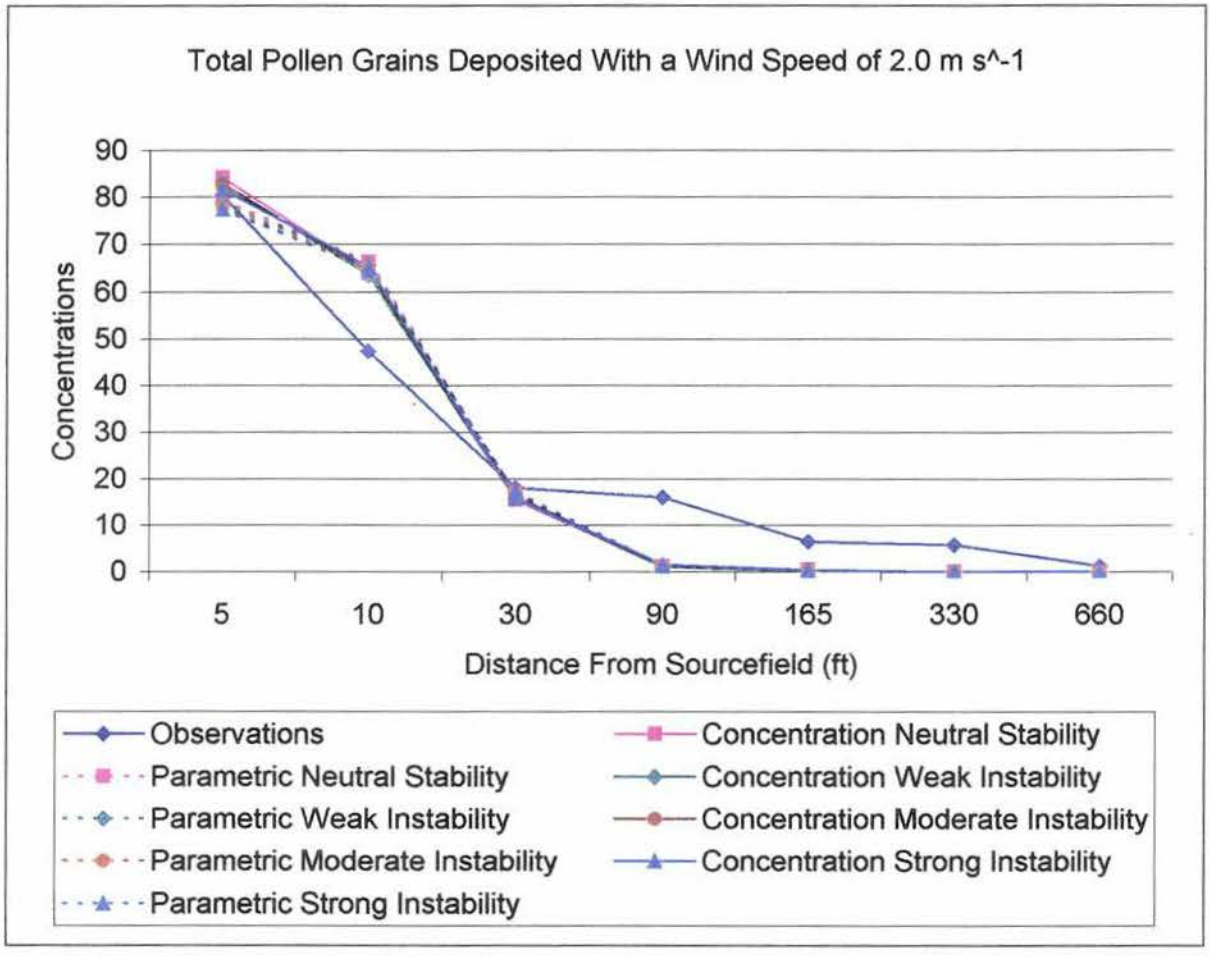

Figure 7.13. The deposition profile of all the axes over the distance away from the source field with a wind speed of 2.0 m s^{-1}. The deposition is given in cm^{-2}.

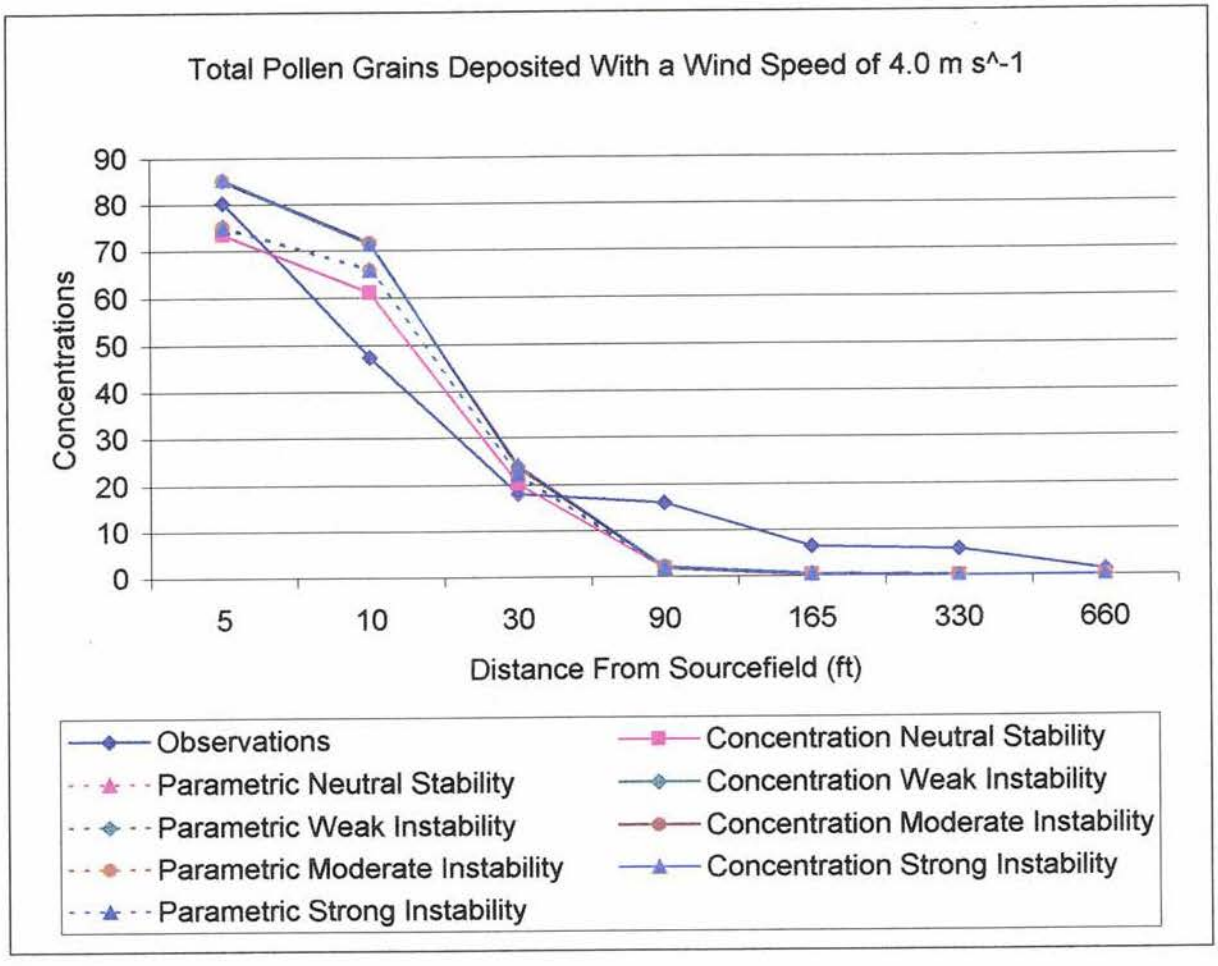

Figure 7.14. The deposition profile of all the axes over the distance away from the source field with a wind speed of 4.0 m s^{-1}. The deposition is given in cm^{-2}.

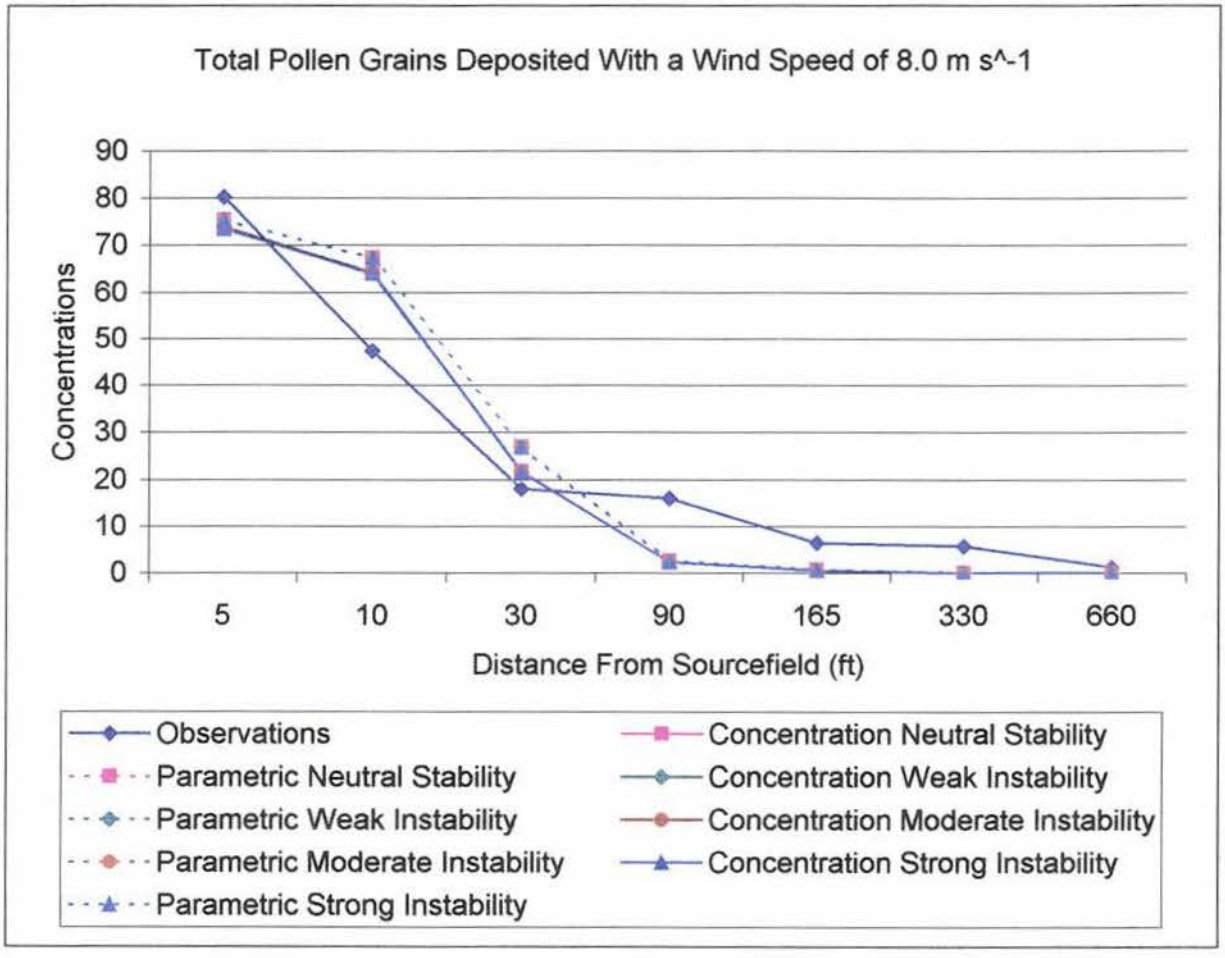

Figure 7.15. The deposition profile of all the axes over the distance away from the source field with a wind speed of 8.0 m s^{-1}. The deposition is given in cm^{-2}.

CHAPTER 8. CONCLUSIONS AND FUTURE WORK

This study found that the Lagrangian Pollen Dispersion Model was able to predict the direction and concentration of maize pollen. The concentration values did not match up with the observations exactly, but in general the model predicted pollen where the observations showed pollen concentration. The Lagrangian Pollen Dispersion Model gave similar results with the Gaussian model ISCST3. Both of these models varied little with observations. One difference the models had from the observations is that they were able to show pollen concentrations in between the axes (north, south, northeast, ect.) and the observations were not able to. This made it possible for the models to predict pollen dispersion downwind of the source field, where most of the pollen grains will be deposited.

Pollen dispersion is sensitive to pollen grain size. Larger pollen grains land closer to the source field because of the larger terminal fall speed associated with the pollen grains; smaller pollen grains land farther from the source field because of the smaller terminal fall speed associated with them. Using a pollen size distribution in the model runs matched up the best with observations. This shows that a pollen size distribution should be used when accounting for pollen terminal fall speed. Not every pollen grain is made equal; some are smaller and some larger than the average.

Sensitivity tests on wind speed and atmospheric stability showed that stronger wind speeds caused the pollen grains to land farther from the source field than lighter wind speeds and that stronger instability also caused pollen grains to land farther from the source field than under neutral or weak instability conditions. When the wind speeds increased to 2 m s^{-1} or more, the atmospheric stability did not change the distribution of the pollen grains. When the wind speeds were less than 2 m s^{-1}, with increasing atmospheric instability the pollen grains traveled farther from the source field.

Some things could be changed to make the pollen dispersion model match up better with observations. One of these changes can be to add more variability with the wind speed and direction.

The weather observations we have from the summer of 2000 are fifteen minute wind speed and direction. It would be appropriate to use these data at fifteen minute intervals instead of averaging them to use one wind speed and direction for each hour. Another change that can be made is to add more layers in the model to account for the corn canopy. One of the biggest problems with the pollen dispersion model is that it does not have the pollen travel as far as it should. One way that could help this problem is to allow for the pollen grains that get deposited on the ground to be picked up (i.e. resuspended) again so they can get carried farther downwind.

More observations are needed to verify the Lagrangian Pollen Dispersion Model more accurately. It would be helpful to have more observation values at distances farther away from the source field since the main interest in this study is in pollen outcross. It would also be useful to put more receptors downwind (and not at just on the eight major axes of north, northeast, east, etc.) each day so that data can be compared where the concentrations are the greatest.

REFERENCES

Ashton, B. A., D. S. Ireland, M. E. Westgate, 2000: Applicability of the Industrial Source Complex (ISC) Air Dispersion Model for use on corn pollen transport. thesis, Dept. of Geological and Atmospheric Sciences, Iowa State University, 11 pp. [Available from Iowa State University, Department of Geological and Atmospheric Sciences, 3010 Agronomy Hall, Iowa State University, Ames, IA 50011.]

Aylor, D. E. and T. K. Flesch, 2001: Estimating spore release rates using a Lagrangian stochastic simulation model. *J. Appl. Meteor.*, **40,** 1196-1208.

Bassetti, P. and M. E. Westgate, 1993a: Emergence, elongation, and senescence of maize silks. *Crop Sci.*, **33,** 271-275.

_____ and _____, 1993b: Water deficit affects receptivity of maize silks. *Crop Sci.*, **33,** 279-282.

_____ and _____, 1994: Floral asuncrony and kernel set in maize quantified by image analysis. *Agron. J.*, **86,** 699-703.

Bonnett, O. T., 1966: *Inflorescences of Maize, Wheat, Rye, Barely, and Oats.* University of Illionios, College of Agriculture, Agriculture Experiment Station Bulletin, 721 pp.

Cionco, R. M., 1972: A wind-profile index for canopy flow. *Boundary-Layer Meteor.*, **3,** 255-263.

Coceal, O. and S. E. Belcher, 2003: A canopy model of mean winds through urban areas. *(Submitted to Q. J. Royal Meteorol. Soc.)*

Emberlin, J., B. Adams-Groom, and J. Tidmarsh, 1999: A Report on the Dispersal of Maize Pollen. [Available on-line from http://www.mindfully.org/GE/Dispersal-Maize-Pollen.UK.htm]

Finnigan, J., 2000: Turbulence in plant canopies. *Annu. Rev. Fluid. Mech.*, **35,** 519-571.

Garratt, J. R., 1992: *The Atmospheric Boundary Layer*. Cambridge University Press, 316 pp.

Herrero, M. P. and R. R. Johnson, 1980: High temperature stress and pollen viability of maize. *Crop Sci.*, **20,** 796-800.

Hogstrom, U., 1996: Review of some basic characteristics of the atmospheric surface layer. *Boundary-Layer Meteor.*, **78,** 215-246.

Kiesselbach, T. A., 1999: *The Structure and Reproduction of Corn. 50th Anniversary Edition.* Cold Springs Harbor Press, 101 pp.

Loubet, B., N. Jarosz, B. Durand, X. Foueillassar, and L. Huber, 2002: Measured airborne concentration and deposition rate of maize pollen (*Zea mays* L.) downwind of an experimental field. Preprints, *25th Conference on Agricultural and Forest Meteorology,* Norfolk, VA, Amer. Meteor. Soc., 24-25.

Luna, S. V., J. M. Figueroa, B. M. Baltazar, R. L. Gomez, R. Townsend, and J. B. Schoper, 2001: Maize pollen longevity and distance isolation requirements for effective pollen control. *Crop Sci.*, **41,** 1551-1557.

Mahrt, L., 1997: Surface fluxes and boundary layer structure. *Clear and Cloudy Boundary Layers,* A. A. M. Holtslag and P. G. Duynkerke, Royal Netherlands Academy of Arts & Sciences, 113-128.

McNider, R. T., 1981: Investigation of the impact of topographic circulations on the transport and dispersion of air pollutants. Ph.D. dissertation, University of Virginia, Charlottesville.

Molder, M., A. Grelle, A. Lindroth, and S. Halldin, 1999: Flux-profile relationships over a boreal forest – roughness sublayer corrections. *Agric. For. Meteor.*, **98-99,** 645-658.

Nathan, R., 2002: Mechanisms of long-distance dispersal of seeds by wind. *Nature,* **418,** 409-413.

National Corn Growers Association cited 2001: You can count on corn. [Available on-line from http://www.ncga.com/education/unit1/u113.html.]

Oke, T. R., 1979: *Boundary Layer Climates.* Wiley & Sons, 372 pp.

Raupach, M. R., J.J. Finnigan, and Y. Brunet, 1996: Coherent eddies and turbulence in vegetation canopies: the mixing-layer analogy. *Boundary-Layer Meteor.*, **78,** 351-382.

Raynor, G. S., E. C. Ogden, and J. V. Hayes, 1972: Dispersion and deposition of corn pollen from experimental sources. *Agron. J.*, **64,** 420-427.

Schoper, J. B., R. J. Lambert, and B. L. Vasilas, 1987: Pollen viability, pollen shedding, and combining ability for tassel heat tolerance in maize. *Crop Sci.*, **27,** 27-31.

Shaw, R. H., R. H. Silversides, and G. W. Thurtell, 1974a: Some observations of turbulence and turbulent transport within and above plant canopies. *Boundary-Layer Meteor.*, **5,** 429-449.

Shaw, R. H., G. Den Hartog, K. M. King, and G. W. Thurtell, 1974b: Measurements of mean wind flow and three-dimensional turbulence intensity within a mature corn canopy. *Agric. Meteor.*, **13,** 419-425.

Uliasz, M., 1993: The atmospheric mesoscale dispersion modeling system. *J. Appl. Meteor.*, **32,** 139-149.

Westgate, M. E., J. Lizaso, and W. Batchelor, 2003. Quantitative relationships between pollen shed density and grain yield in maize. *Crop Sci.*,**43,** 934-942.

Wilson, J. D., 2000: Trajectory models for heavy particles in atmospheric turbulence: comparison with observations. *J. Appl. Meteor.*, **39,** 1894-1912.

_____, D. P. Ward, G. W. Thurtell, and G. E. Kidd, 1982: Statistics of atmospheric turbulence within and above a corn canopy. *Boundary-Layer Meteor.*, **24,** 495-519.

Wilson, N. R., and R. H. Shaw, 1977: A higher order closure model for canopy flow. *J. Appl. Meteor.*, **16,** 1197-1205.

ACKNOWLEDGEMENTS

I would like to acknowledge and thank the many people who helped me accomplish this thesis. My husband, Brent Riese, who was of great support to me, not only did he listen to my problems and concerns with the thesis, he made me dinner so I could continue my work in the evening. My parents, sister, and parents-in-laws for their encouragement and continuing support. The rest of my family was also a great support, especially Paul Teig, who dug up some corn articles (that I just had to read!) for me twice (including the day before I presented my thesis!).

A huge thank you to Dr. Ray Arritt (for being a great mentor and advisor), Dr. Mark Westgate (for teaching me more than I ever wanted to know about corn) and Dr. Gene Takle (for the encouragement to continue on to grad school). I would also like to thank the rest of the agricultural meteorology and meteorology professors for all of their encouragement through both my undergraduate and graduate years.

I would also like to thank all of my officemates (Chris, Jimmy, Darren, and Craig) for putting up with me through the past couple years and helping me out with meteorology and programming questions. And finally, a thank you to all of the meteorology students for all of their help and support.